'Overthickening' of Sedimentary Sequences by Igneous Intrusions

[1]NIALL MARK*, [1]NICK SCHOFIELD, [2]DAVID GARDINER, [3]LIAM HOLT, [3]CLAYTON GROVE, [1]DOUGLAS WATSON, [3]ANDY ALEXANDER, [3]HEATHER POORE

[1]Department of Geology and Petroleum Geology, University of Aberdeen, Aberdeen AB24 3UE, UK

[2]Integrated Geochemical Interpretation Ltd, The Granary, Hallsannery, Bideford, Devon, EX39 5HE, UK

[3]Siccar Point Energy Limited, Hill of Rubislaw, Anderson Drive, Aberdeen, AB15 6BY, UK

**Corresponding author (e-mail: niall.mark@abdn.ac.uk)*

ABSTRACT

The identification of extensive intrusive igneous complexes both in subsurface data and in field studies has resulted in quantification of the volumes of igneous material. Despite this research there is still little connection established between the amount of igneous material intruded into a basin and its effect on subsequent basin evolution in terms of burial and loading. To understand how additional igneous material may influence basin evolution we investigate igneous intrusions from the Faroe-Shetland Basin (FSB) utilising subsurface data. This study highlights that the total estimated thickness of sediment during Cretaceous is likely an overestimate as the sedimentary fill consists of significant quantities of igneous material which was emplaced during the Paleocene (56-54 Ma).

Previously this additional igneous material has not been accounted for in estimates of sedimentation rates and the burial history of the FSB. Importantly petroleum system modelling to understand generation and expulsion of hydrocarbons benefits from correct estimates of basin fill. The overthickening of basins by igneous material will affect the timing of hydrocarbon generation and subsequently the proper evaluation of exploration targets. In order to fully understand basin evolution the volumes of igneous material and when this material was emplaced must be acknowledged and considered.

INTRODUCTION

Research of igneous intrusion and magma movement within the shallow crust has benefited greatly in recent years from the utilisation of three dimensional (3D) seismic reflection datasets acquired for hydrocarbon exploration. These datasets have allowed for detailed analysis of basins with igneous intrusions globally, with studies identifying emplacement mechanisms, intrusion morphologies and the impacts of the intrusions on hydrocarbon exploration (Davies *et al.* 2002; Smallwood & Maresh 2002; Thomson and Hutton 2004; Planke *et al.* 2005; Archer *et al.* 2005; Holford *et al.* 2013; Schofield *et al.* 2015; Mark *et al.* 2017). Recent studies have focused on marrying field observations with subsurface data which has broadened the understanding of intrusive igneous processes (Schofield *et al.,* 2012a, Eide *et al.,* 2017a; Eide *et al.* 2017b). Commonly research into igneous intrusions has attempted to determine the total volume of the intrusive material by using subsurface data and also field based studies (Smallwood & Maresh 2002; Svensen *et al.* 2012; Richardson *et al.* 2015; Reynolds *et al.* 2018). By determining the total volumes of intrusive igneous material, researchers have attempted to predict factors such as extrusive effusion rates, mechanisms driving volcanism, dimensions of shallow magma chambers and intrusive to extrusive ratios (Ellwood & Watkins 1976; White *et al.* 2006; Valentine & Perry, 2007; Ferguson *et al.* 2010; Richardson *et al.* 2015; Reynolds *et al.* 2018).

Previous studies from other basins with significant intrusive igneous material have estimated, using a variety of methods, the total volumes of intrusive igneous material. The Karoo Basin, South Africa is estimated to contain 340,000 km^3 of intrusive igneous material based on geology maps (Svensen *et al.* 2012). Within the Northern Atlantic Margin, 560 – 780 km^3 of igneous material has been revealed from deep penetration seismic profiles along the continent-ocean transition (Roberts *et al.* 2009). Additionally, in the Bight Basin, Southern Australia, 92 - 111 km^3 of intrusive igneous material was calculated from seismic mapping of 3D seismic data (Reynolds *et al.* 2018).

Although it has been observed that the emplacement of igneous intrusions into a sedimentary basin can result in localised forced folding of the overburden, host rock deformation and compartmentalisation of sediments (Gibb & Kanaris-Sotiriou 1988; Bell & Butcher 2002; Archer *et al.* 2005; Thomson & Schofield 2008; Schofield *et al.* 2015; Magee *et al.* 2016; Grove *et al.* 2017; Senger *et al.* 2017), the critical link between magmatic intrusion into a sedimentary basin and the implication for

58 a basin's evolution has yet to be made. Recent work in basins with extensive igneous intrusions has
59 also highlighted problems related to understanding what igneous material is not being seismically
60 imaged in the subsurface due to issues such as the vertical resolution of both well and seismic data
61 (Schofield *et al.* 2015; Eide *et al.* 2017b; Mark *et al.* 2017). Work by Schofield *et al.* (2015) and Mark *et*
62 *al.* (2017) revealed that >80% of the intrusions within the Faroe-Shetland Basin (FSB) (and likely other
63 basins globally) would not be imaged due to the igneous intrusions being of a thickness significantly
64 below that needed to resolve in seismic reflection data.
65 To evaluate the impact of this additional igneous material on basin evolution we have
66 interpreted 143 igneous intrusions in 3D seismic datasets from the FSB and estimated the thickness
67 and total volume of intrusive material (Fig. 1). The major findings of this work are: : (1) the total
68 volume of mafic intrusive igneous material within the study ranges from a minimum of 399 km^3 to a
69 maximum estimate of 2,300 km^3; (2) the distribution of this additional igneous material is highly varied
70 across the FSB, and ranges from 20 m (Southern Flett sub-basin) to over 1.8 km (Nuevo sub-basin);
71 (3) critically, the additional igneous material has resulted in an overestimation of sedimentary thickness
72 across large areas of the FSB; (4) basin modelling for the FSB should compensate for the over
73 thickening of the sedimentary fill by igneous material during sediment deposition and incorporate it at
74 the appropriate time.
75 We believe that these insights present a vital methodology to fully understand how significant
76 volumetric input of intrusive igneous material can impact estimations of the scale of magmatic activity,
77 sedimentation rate and the general basin evolution.
78
79 **GEOLOGICAL HISTORY**
80 The FSB is located between the Faroe and Shetland Islands on the Atlantic passive continental margin
81 of NW Europe (Fig. 1). The basin can be sub-divided into a series of SW-NE trending sub-basins and
82 is bound by the Rockall Trough to the SW and the Møre Basin to the NE (Hitchen & Ritchie 1987).
83 The sub-basins consist of Mesozoic to Recent sediments bounded by basement highs comprised of
84 Precambrian crystalline rocks capped by Palaeozoic and Mesozoic sediments (Lamers & Carmichael

1999). The FSB has undergone several stages of rifting between the Devonian and Paleocene, followed by Cenozoic episodes of inversion (Smallwood & Maresh 2002; Ritchie *et al.* 2011; Ellis & Stoker, 2014).

The FSB, along with the NE Atlantic Margin, underwent considerable igneous activity during the late Paleocene to Early Eocene (White & Mckenzie 1989; Jolley & Bell 2002; Ellis & Stoker 2014; Hardman *et al.* 2018). This igneous activity resulted in expulsion of extensive extrusive basaltic sequences and the emplacement of a pervasive suite of sills and dykes, the majority of which intrude into Upper Cretaceous shales (Gibb & Kanaris-Sotriou 1998, Bell & Butcher 2002, Thomson & Schofield 2008, Schofield *et al.* 2015, Schofield *et al.* 2017). The assemblage of sills and dykes are collectively termed the Faroe-Shetland Sill Complex (FSSC) and are identified throughout the SW-NE trending sub-basins of the FSB, extending northwards into the Møre basin and southwards into the Rockall Trough (Ritchie *et al.* 2011; Schofield *et al.* 2017) (Fig. 1).

DATASET

The data used within this study consists of the Faroe-Shetland PGS MegaSurvey Plus and the PGS/TGS FSB 2011-12 MultiClient GeoStreamer, 3D seismic datasets (Fig. 1b). The MegaSurvey Plus covers an area of 24,000 km^2 and the FSB 2011-12 survey covers an area of 2,662 km^2. The MegaSurvey Plus data has undergone substantial reprocessing leading to improved imaging of the FSSC (Schofield *et al.* 2015). The FSB 2011-12 data were acquired using Geostreamer technology which records broader bandwidth than were possible with older conventional data. The preservation of lower frequencies is critical for imaging the FSSC below the extrusive basalt towards the west of the study area (Hardman *et al.* 2018). Both of the 3D datasets are displayed in the time domain only and are displayed at standard polarity (Sheriff & Geldart 1995), with a downward increase in acoustic impedance corresponding to a positive amplitude (hard kick), displayed in red, and a downward decrease in acoustic impedance corresponding to a negative amplitude (soft kick), displayed in blue (Fig. 2). The igneous intrusions which were mapped across the study area were interpreted on a positive amplitude

(red) (Fig. 2). The intrusions are readily identified as high amplitude features which are laterally discontinuous and cross-cut stratigraphy.

The well data includes all the released exploration and appraisal wells drilled in the FSB, which were analysed to identify igneous intrusions (see Mark *et al.* 2017). Within this dataset, 30 wells encountered intrusions with 252 penetrations of individual intrusions. For each intrusion the thickness and host rock lithology and age was recorded. The locations of the wells that encountered igneous intrusions are highlighted in Fig. 1. Despite the location of some wells outside the main study area, they were still used to scale the interpreted seismic intrusive data and infer relationships that are not possible at the resolution of seismic data (see below).

CALCULATING THICKNESS AND VOLUME OF IGNEOUS INTRUSIONS IN SEISMIC DATA

Method for calculating the thickness and volume of individual intrusions

To estimate the total volume of the igneous material within the study, the area of each intrusion was first determined by seismic mapping and the area multiplied by the thickness of each igneous intrusion. With only six wells in the study area that penetrate igneous intrusions it is not possible to determine the thickness of each individual intrusion using well data, so a method to calculate thickness from seismic data had to be developed.

To calculate the thickness of multiple igneous intrusions across the FSB in seismic data we utilise a tuning wedge model (Widess 1973; Simm & Bacon 2014) combined with conventional depth conversion where igneous intrusions are imaged in seismic data. As specified by Smallwood & Maresh (2002), Schofield *et al.* (2015), and Mark *et al.* (2017), the majority of intrusions in the FSB have thicknesses that result in them being imaged as tuned reflectors (where reflections from the top and base of the intrusion constructively interfere to form a single reflector/wavelet). Of the 145 intrusions mapped in this study, only 2% are fully resolvable with a clear top and base reflector, while the remaining 98% of the mapped intrusions are imaged as tuned reflectors only (Fig. 2). For the fully resolved intrusions it is possible to map the top and base of the intrusion, and these are depth converted using a velocity of 5,500 meters per second (m/s) (determined from sonic logs in wells that

139 penetrate basaltic igneous intrusions in the FSB) to calculate the thickness between the top and base
140 intrusion surface (Fig. 3).

141 When an undrilled igneous intrusion is seen within seismic data as a tuned reflector, it is not
142 possible to determine the thickness precisely. Instead the upper and lower range of the intrusion
143 thickness can be defined. The maximum thickness of the intrusion is defined by the tuning thickness
144 (1/4 wavelength) since above this thickness, the top and base of the intrusion would become visible as
145 distinct seismic events, and the reflection would no longer be tuned. The minimum thickness of an
146 intrusion has been defined here by the detection limit of the seismic data (i.e. the thickness at which
147 the amplitude merges with the background), below which the intrusion would not be detected in the
148 seismic data (Fig. 3). This therefore gives a maximum and minimum thickness range for intrusions
149 represented by a tuned reflector.

150 To determine the tuning thickness of the data and the limit of detectability, first the frequency
151 of the seismic data for the area of interest, and second, the depth where the intrusions occur, must
152 be ascertained. The dominant frequency was obtained for each individual intrusion imaged in the
153 seismic data. This allowed changes in dominant frequency, as a result depth of emplacement,
154 differences in the overburden and different surveys, to be accounted for across the study area.

155 Using the dominant frequency of the seismic data close to the intrusion and the average
156 interval velocity of the intrusions (determined from wells which encountered intrusions) the seismic
157 wavelength is calculated using the formula, $\lambda = V/f$, (λ: Lambda, seismic wavelength in m) (V: interval
158 velocity, in m/s), (f: seismic frequency in Hz) (Widess 1973; Simm and Bacon 2014). The limit of
159 detectability of seismic reflection data is variously quoted as being between $\lambda/30$ and $\lambda/8$, and the limit
160 of resolution is $\lambda/4$ (Widess 1973). It is important to note that these limits are very much 'rules of
161 thumb' and are unique to any given seismic dataset, being affected by factors such as signal to noise
162 ratio, acquisition and processing (Eide *et al.* 2017b). To ascertain what tuning thickness and
163 detectability limit to use for igneous intrusions mapped within this study we examined wells within
164 both surveys that penetrated both thick, seismically resolvable, and thin, unimaged intrusions.

For example, well 205/10-2B encountered 44 intrusions in total (determined from wireline logs and formation logs), ranging in thickness from 1 m to 48 m. Based on the seismic data through this well, only three of these intrusions are identifiable as discrete reflectors within the seismic data (Fig. 4). These intrusions are 36, 48, and 49 m thick respectively. However, the 36 and 49 m thick intrusions are actually four closely spaced intrusions constructively interfering to produce a response (Fig. 4). The other 39 intrusions penetrated by the well are not detectable in the seismic data (Fig. 4). This suggests that within the seismic data alone, intrusions which are below 36 m in thickness are not detected.

By applying the tuning wedge thickness method to intrusions detected in seismic at the location of wells which encountered igneous intrusions we can test the viability of λ/4, λ/8 and λ/30 for assessing the thickness of intrusions in the seismic data, given we know the true and absolute intrusion thicknesses from the well logs (Fig. 4). Using well 205/10-2B as an example, at the location of the well, the dominant frequency of the seismic data is 15.9 Hz in the region of the intrusion penetrations. We calculate thicknesses for the igneous intrusions between the tuning thickness (λ/4) as 86 m, and seismic detectability (λ/8) as 43 m or 11.5 m for λ/30.

From these results we determined that λ/4 for the tuning thickness and λ/8 for the limit of detectability was the most suitable representation of what could be seen within the seismic data, as the range of thickness λ/4 and λ/8 calculates for the tuned reflectors (i.e. 86 m and 43 m respectively) is comparable to the true thickness of the imaged intrusions in the well (48m, 36 and 49m), indicating that these methods accurately predict the upper and lower range of thickness of tuned reflectors in the seismic data. (Fig. 4).

Although λ/30 is often quoted as the limit of detectability within seismic reflection datasets (Eide *et al.* 2017b), we found this would typically underestimate the thickness of the intrusions considerably, compared with its true thickness in the well (Fig. 4). In addition, the thickness estimate that λ/30 provides would indicate that all 44 intrusions encountered by 205/10-2B should, in theory, be detected in the seismic data, which is clearly not the case, as only three clear intrusive reflectors are visible in the seismic data (Fig. 4). This was also noted by Eide *et al. (*2017b) who observed that

192 even for good quality seismic data (such as that data used in this study) typical detectability limits of
193 λ/30 are unlikely due to factors such as signal to noise ratio and properly accounting for the complexity
194 of the subsurface velocity model during processing.

195 Having assessed the suitability of the tuning wedge model it is then possible to calculate a
196 range of thicknesses for each intrusion with λ/4 (tuning thickness) producing a maximum estimate and
197 λ/8 (limit of detectability) producing a minimum estimate. This thickness calculation assumes the
198 intrusion is one thickness in the seismic data, which is an obvious simplification, as from field
199 observations it is known that intrusions generally thicken and thin across their full body (e.g. field
200 outcrops of sill complexes Jameson Land, East Greenland (Eide *et al.* 2017a)). However, by calculating
201 a minimum and maximum thickness we constrain this variability in intrusion thickness across the full
202 intrusive body. The total volume of igneous material was then calculated by summing the volume of
203 igneous material for each igneous intrusion.

204

205 *Scaling the data to account for intrusions below seismic resolution*

206 Due to the limits of vertical resolution, igneous intrusions cannot often be detected in seismic data,
207 which can, cumulatively, account for a substantive thickness in a subsurface sedimentary sequence
208 (Schofield *et al.* 2015; Eide *et al.* 2017b; Mark *et al.* 2017). In areas of direct well control, this is not an
209 issue, as the unimaged intrusion thicknesses can be taken directly from well log interpretation.
210 However, in areas where igneous intrusions are imaged on seismic reflection data but without direct
211 well correlation, a methodology needs to be employed to take into account the thickness of seismically
212 unimaged intrusions.

213 For all six wells that penetrated igneous intrusions in the study area we have determine from
214 petrophyscial data and formation logs that there is a total thickness of 504 m of igneous material.
215 Some of this material has been discounted as the 205/10-5A well encountered a 90 m thick silicic
216 igneous intrusion which is not representative of the main FSSC, the majority of which consists of
217 basaltic material (Mark *et al,* 2017). The total thickness of igneous material is therefore 414 m, of this,
218 177 m of this material is seismically resolvable. The remaining 237 m is not detected in the seismic

219 data, which gives a ratio of 1:1.4 for the amount of seismically detectable igneous material to
220 undetected igneous material. Figure 5 determines how we determined this ratio using the example of
221 the 205/10-2B well, which was then applied to all the wells that encountered igneous intrusions within
222 the study area. By using this relationship it could be argued that, for example, for a given 50 m thick
223 intrusion there is potentially another 70 m cumulative thickness of undetected intrusive material, in
224 the form of numerous <1-10's m thick sills. Figure 6 demonstrates the application of the 1:1.4 ratio
225 obtained from the well data to regions with no well penetrations to constrain how much igneous
226 material is potentially missing in the seismic data (Fig. 6).
227
228 **RESULTS**
229 *Overview of igneous intrusions in the study area*
230
231 The mapped intrusions have an aerial extent of 10,500 km^2. In total, 145 individual igneous intrusions
232 were interpreted across the study area (Fig. 7), with individual intrusion areas ranging from 1 km^2 to
233 1,000 km^2. The majority of the mapped intrusions are hosted within the Upper Cretaceous (111
234 intrusions out of a total of 145 intrusions, 76.5%). Of the remaining 34 intrusions, 19 occur in the
235 Lower Cretaceous (13.1%), 12 in the lower Paleocene (8.2%) and the remaining three in the Upper
236 Jurassic (2%). The dominance of intrusions into Cretaceous strata versus Paleocene strata is clear, due
237 to the preferential exploitation of argillaceous sequences (Mark *et al.* 2017). However, it should be
238 noted that due to the degradation in seismic quality below the Cretaceous sequences caused by the
239 numerous intrusions, the apparent drop in intrusion frequency in older strata (e.g. Jurassic) is
240 potentially a function of attenuation and a reduction in seismic bandwidth and the signal to noise ratio
241 of the data.
242 Across the study area, the majority of intrusions can be seen to occur within sub-basins, with
243 the greatest proportion of the intrusions seen within the Nuevo and Flett sub-basins, where heavily
244 intruded Upper Cretaceous sections are observable (Fig. 7). The basinal highs typically have fewer
245 igneous intrusions. The Flett and Rona Ridges have abundant igneous intrusions, through sections,
246 likely due to their proximity to major bounding faults and lineaments (Schofield *et al.* 2015).

247 Importantly, the wells that penetrated igneous intrusions were drilled on the basinal highs, and have
248 fewer numbers of igneous intrusions than the basins, based on seismic observations.
249 The morphology of the mapped intrusions is variable, with the majority of the intrusions having
250 a saucer-shaped morphology, similar to those outlined in Smallwood & Maresh (2002) and Bell &
251 Butcher (2002). However, in the Nuevo sub-basin (Fig. 7) the intrusion morphologies bifurcate and
252 interconnect, crosscutting the host rock stratigraphy, similar to the chaotic morphologies described
253 onshore Greenland by Eide *et al.* (2017a).
254
255 *Thickness and Volume Estimates for Imaged Igneous Intrusions*
256 Using seismically imaged intrusions alone, thicknesses for 145 igneous intrusions were calculated. The
257 average thickness of all the intrusions in the study area for the maximum (λ/4) and minimum estimate
258 (λ/8) is 92 m and 42 m respectively (Fig. 7). Based on these thickness estimates, apparent thickness
259 maps (isopach) for every mapped intrusion have been created across the full study area, which show
260 the cumulative thickness of igneous intrusive material for the minimum and maximum scenarios (Fig.
261 7).
262 Areas of multiple stacked intrusions have been observed, such as in the Nuevo and Flett sub-
263 basins where the cumulative thicknesses of imaged igneous material can be as great as 850 m, taking
264 the maximum thickness estimates (λ/4), and as little as 500 m using the minimum estimate (λ/8) (Fig.
265 7). In other regions of the study area where no intrusions have been imaged the cumulative thickness
266 maps show no igneous material. However, undetectable sills are likely to be present in these areas
267 (Fig. 7).
268 For the volume of igneous material for each mapped igneous intrusion, we determined a range
269 of volumes based on the maximum (λ/4) and minimum (λ/8) thickness estimates. For the maximum
270 (λ/4) thickness estimate the volumes of the individual igneous intrusions ranges from 205 km^3 to 0.05
271 km^3 with an average volume of 6 km^3. For the minimum (λ/8), thickness estimate the volumes of the
272 individual igneous intrusions ranges from 41 km^3 to 0.02 km^3 with and average volume of 2 km^3. It is
273 worth noting that the upper ranges of thickness and volume is skewed by one anomalously thick and

laterally extensive igneous intrusion in the north of the study area which has an individual area of 1,002 km^2, but is potentially much larger as its total extent is outside of the study area. The cumulative volume of all the igneous material across the study area when taking the maximum and minimum thickness estimates ranges from 399 – 925 km^3.

Thickness and volume estimates for imaged & the addition of unimaged igneous intrusions

Although the thickness and volume ranges calculated in the previous section can give a first order approximation of igneous material within the FSB, they do not, as discussed in the methodology section, take into account the thickness (and volume) of seismically undetectable igneous intrusions.

Using the ratio of 1:1.4 of imaged to unimaged intrusions, we have also created thickness maps which show the cumulative thickness of intrusive igneous material, similar to the maps outlined above, but scaled to account for unimaged igneous material (Fig. 7). For these cumulative thickness maps in areas with multiple stacked intrusions, such as the Nuevo sub-basin, the cumulative thickness of igneous material is as great as 850 m based on the mapped visible intrusions, however taking into account unimaged intrusions our study implies there is potentially cumulative thicknesses of 2,000 m (Fig. 7). Figure 8 shows the intrusion thickness maps in the context of the basin structure demonstrating the greater abundance of igneous intrusions in region such as the Nuevo sub-basin (Fig. 8).

We have also determined a range of volumes based on the maximum (λ/4) and minimum (λ/8) thickness estimates including the addition of the unimaged intrusions. The cumulative volume the igneous material across the study area, taking the maximum and minimum thickness estimates plus the addition of seismically unimaged igneous material, ranges from 957 – 2,220 km^3.

DISCUSSION

Accounting for the underestimations of igneous material

The cumulative thickness and volume of igneous material discussed is based on the mapping of intrusions in seismic data and scaling this to account for the thin intrusions that cannot be detected in

seismic data. Utilising well logs to calibrate seismic interpretations across the study area our method provides a good estimate of the range of igneous material thicknesses and volumes but it is *still* likely to underestimate the total volume of igneous material within the basin due to factors such as vertical to sub-vertical intrusions and intrusions with variable compositions (e.g. lower acoustic impedance silicic intrusions).

The intrusions that have been mapped across the study area are all identified as horizontal to sub-horizontal features, classifying them as sills. Vertical features, such as igneous dykes, are inherently difficult to image in seismic data. However, field observations from other basins with igneous intrusions imply ratios of sills to dykes of 1:166 (San Rafael, south west Utah, San Rafael Intrusive Complex (Kyosugi *et al.* 2012)) to 1:3 (lower Paleogene intrusive complex on Jameson Land, East Greenland (Eide *et al.* 2017a)). The type of intrusion morphology is largely controlled by the tectonic regime, therefore extensional basins are commonly associated with vertical features such as dykes. Although these studies demonstrate that dykes are more abundant than sills, the dykes tend to be much thinner and thus account for lower volumes of igneous material.

Mark *et al.* (2017) demonstrated in a study from the FSB that, based on well and seismic data that there are rare occurrences of silicic intrusions (<10% based on well penetrations). These may be underrepresented due to their lower density and compressional sonic velocities when compared to mafic intrusions, meaning they are hard to image in seismic and well data (Mark *et al.* 2017). These silicic igneous intrusions would result in additional igneous material, which cannot be accounted for, further underestimating the amount of igneous material in the basin.

Comparison of total volume of intrusive material to previous estimates

Estimating the volume of igneous material in a basin has importance for understanding the magma productivity through time, deep mantle activity and even climactic drivers (White & Mckenzie 1989; Storey *et al.* 2007; Aarnes *et al.* 2010). To test the validity of the methodology and the values we have calculated, we compare this study's volume of igneous material to previous work looking at the range of volume of igneous material in a basin. Previous estimates of the total volume of igneous material in

330 the North Atlantic Igneous Province (NAIP) range from 5-10 x 10^6 km^3, (White & Mckenzie 1989;
331 Eldholm & Grue 1994; Holbrook *et al*. 2001) which includes both extrusive and intrusive volcanism in
332 the FSB, Rockall, Møre and Vøring Basins and Greenland region (area of 1.3 x 10^6 km^2, Eldholm & Grue
333 1994). These studies calculated their volumes based on limited 2D seismic transects across the NAIP
334 margins and sparse well data obtained from the Ocean Drilling Program (ODP) (White & Mckenzie
335 1989; Eldholm & Grue 1994; Holbrook *et al*. 2001). The total volume of igneous material across this
336 10,500 km^2 study area ranges from 399 km^3 to 2,405 km^3 including the minimum and maximum scaled
337 thickness data. Scaling the volume of intrusive igneous material calculated in this study to the same
338 area of the total NAIP from Eldholm & Grue (1994) produces volumes ranging from 4.9 x 10^4 to 2.9
339 x 10^5 km^3. Despite our lower estimate than the previous work it is likely more accurate given that it
340 is linked to well data and previous studies were dependant on limited well data and sparse 2D seismic
341 data.

342 This study, when compared with research that also primarily focuses on the intrusive igneous
343 material volumes using a similar seismic method have comparable values for the volume of intrusive
344 igneous material. The study by Reynolds *et al*. (2018) for the Bight Basin, Australia, used a similar
345 technique and resulted in igneous volumes of 92-111 km^3 which are comparable considering the scale
346 of the study and number of intrusions in the study area, indicating that the technique also applied in
347 this study is producing valid volume estimates of igneous material. Planke *et al*. (2005) similarly
348 estimated the volume of intrusive igneous material from seismic data in the Vøring and Møre basins,
349 which contains an extension of the FSSC into the Norwegian Margin estimating study the volume of
350 intrusive igneous material to be in the region of 0.9 x 10^4 to 2.8 x 10^4 km^3 for an area of 80,000 km^2.
351 Scaling the data from this study to the same area as the Vøring and Møre Basins study results in a
352 cumulative volume of igneous material ranging from 3.0 x 10^3 to 1.8 x 10^4 km^3. The volumes are
353 considerably higher than the calculated volumes from the FSB study presented here, when scaled to
354 the same area as the Vøring and Møre basin study (Planke *et al.* 2005). This difference is potentially
355 due to differences in the techniques used to estimate the volumes in both studies. Planke *et al.* (2005)
356 calculated the volume by taking the areal extent of the intrusions and then multiplying this by the

thickness of the intruded basin. This technique captures a range of volumes, but is likely an overestimation due to oversimplification, compared to calculating the volume of each mapped intrusion as demonstrated in this study.

Magma accommodation in sedimentary basins: localized host rock deformation vs 1:1 uplift

The intrusion of magma into sedimentary sequences introduces a volume of material which needs to be accommodated in the subsurface rock mass. When magma is emplaced into clastic rocks that are not fully consolidated or cemented by diagenesis and still retain porosity, much of the volume of magma added can be accommodated by localized host rock deformation mechanisms such as pore-space collapse, expulsion of pore fluids and mechanical compaction (Schofield *et al.* 2012b). Any resulting volume that cannot be solely accommodated by these means, is often accommodated by uplift of the overburden above the intrusion (Einsele *et al.* 1980; Jackson *et al.* 2013; Schofield *et al.* 2012b; Magee *et al.* 2013) (Fig. 9).

However, if magma emplacement occurs deeper within a sedimentary basin, where host rocks are compacted and cemented, the host rock that the magma is intruding into will possess little to no ability to accommodate the volume of the magma by localized host rock deformation. In this circumstance, the additional magma volume added can only be accommodated by uplift/and or faulting of overlying rock on a 1:1 basis (Hutton 2009; Jerram *et al.* 2010; Eide *et al.* 2017a) (Fig. 9).

This theoretically implies, that given a series of intrusions, emplaced at the same time at different depths vertically within a basin, differential vertical uplift will occur. Deep seated intrusions will jack up the overlying host rock by equal amounts to their thickness (see Eide *et al.* 2017a), but at shallow basin levels, a certain degree of magma volume could be accommodated by localised host rock deformation, a mechanism termed 'differential vertical intrusion-induced uplift' by Eide *et al.* 2017a.

The exact transition depth where the host rock becomes incapable of deforming to accommodate magmatic intrusions on a localised scale is difficult to estimate. However, the dominant mechanical mechanism whereby emplacement of magma can be accommodated locally is likely via collapse of any available pore space.

384 During normal burial of sedimentary rocks the reduction in porosity is mainly achieved *via*
385 dehydration and compaction, resulting in the re-arrangement of individual grains and resulting collapse
386 of pore space and by chemical dissolution at grain contacts (Allen & Allen 2013). Within shales,
387 porosity drops rapidly, so that a shale with an initial porosity of ~60% at 0 m, under normal burial
388 conditions, by 2 km burial will have approximately ~ 5-25% porosity, and by 4 km the porosity will
389 have dropped to 15% or lower (Allen & Allen 2013). It is worth noting that porosity values for shales
390 when derived from petrophyscial logs are influenced by the bound water which can calculate higher
391 porosity values. Within sandstones, the depositional porosity typically ranges from 39-49%, however
392 at 2-3 km, porosity reduces to 15-25% (Pryor 1973; Allen & Allen 2013).
393 During intrusion, a host rock's ability to deform to accommodate a volume of magma will also
394 be largely controlled by the ability to compact the host rock and cause further porosity reduction on
395 a local scale (Schofield *et al.* 2012b; Eide *et al.* 2017a). For example, a 50 m intrusion intruded at
396 relatively shallow level of 500 m below the paleo-surface in a predominantly claystone dominated
397 sequence, will be intruding into a host rock of ~ 30-40% porosity, and therefore, a maximum 20 m of
398 the 50m thick intrusion could be accommodated by porosity reduction. For the same 50 m thick
399 intrusion intruded at ~5.5 km depth, the porosity of the host rock, if it has gone through normal
400 compaction, will be in the region of 5-10% with only ~ 2.5 m vertical thickness of the 50 m thick
401 intrusion accommodated *via* host rock compaction. Sandstones typically preserve porosity to greater
402 depths (Gluyas & Cade 1997; Allen & Allen 2003) indicating a higher proportion of igneous intrusion
403 accommodation will occur *via* localised host rock deformation. However, contradictory to this, recent
404 work by Grove (2014) has shown that porosity reduction in sandstones surrounding igneous intrusions
405 is minor and the effects were detected at a maximum of 4 m from the igneous intrusion, indicating
406 that even in porous sandstones local deformation processes will only account for a minor amount of
407 intrusion accommodation. By calculating the paleo-depth of emplacement for the igneous intrusions
408 in the study area we can determine if host rock deformation or 1:1 uplift is the more dominant process,
409 which is important for understanding how the additional igneous material influences basin evolution.

The dominant intrusion accommodation process in the study area was derived from decompaction to calculate the paleo-depth of emplacement for the igneous intrusions across the study area and compare this with compaction curves for the host rock sediments. If the porosity of the host rock sediments is significantly reduced, the ability for the intrusion to be accommodated by host rock deformation is less and 1:1 uplift of the host rock would be the favoured mechanism. To calculate this, we use porosity depth trends for shales (Fig.10) as opposed to sandstones as the majority of the FSSC intrusions are emplaced into the Upper Cretaceous. This unit is composed of thick shale sequences, and from the well data, 97 % of the intrusions penetrated by wells in the Upper Cretaceous are hosted within shale sequences (Mark *et al.* 2017) (Fig. 10).

To determine the paleo-depth of emplacement we utilised a methodology from Smallwood & Maresh (2008) and the decompaction method from Hardman *et al.* (2018). This process begins with back stripping the sediments which were deposited post 56.1 Ma using the age determination of the emplacement of FSSC (Schofield *et al.* 2015), before decompacting all the sediments that occur above the average depth at which the intrusions occur in seismic at the time of emplacement. This gives average paleo-depths of emplacement of 867 m for the lower Paleocene hosted intrusions, 2,521 m for the Upper Cretaceous and 3,276 m for the Lower Cretaceous hosted intrusions.

At the paleo-depth of emplacement for the Upper Cretaceous and Lower Cretaceous hosted intrusions, this implies that the porosity (and therefore the ability for the host rock to take up magma volume addition) would have already been dramatically reduced prior to magmatic intrusion (Fig. 10). Specifically, at the paleo-depth of 867 m for emplacement of the lower Paleocene hosted intrusions the host rock porosity is expected to be 12-45%, for the Upper Cretaceous hosted intrusions at 2,521 m the host rock porosity would be 4-25% and for Lower Cretaceous hosted intrusions the host rock porosity would be 3-18%. At paleo-depths of ~2,500 m where a large majority of the intrusions occur, the porosity of shale would be <10%, indicating that accommodation *via* host rock deformation would have been minimal (Fig. 10). Based on the calculation of the paleo-depth of emplacement we determine that, little to none (<10%) of the intruded igneous volume within the study area would have been able to be accommodated by localized host rock deformation processes. Therefore the emplacement of

magma must have been accommodated by uplift and thickening of the sequences into which they intruded, as per the mechanism proposed by Eide *et al.* (2017a).

Overestimation of the Cretaceous sedimentary fill due to igneous intrusions

If magma intruding into a basin cannot be accommodated by localized host rock deformation, this may create a somewhat geologically unique scenario where a sedimentary unit or sequence can become artificially thickened ('overthickened') post-deposition as a result of intrusion of large volumes of igneous intrusions (Schofield *et al.* 2017). This means that the present day thickness of sedimentary sequences (e.g. Cretaceous) as mapped and ascertained from seismic data across a heavily intruded sedimentary section, will appear to be thicker than originally deposited. In such a circumstance, to determine the true thickness of the sedimentary unit prior to intrusion, the thickness of the intrusions needs to be removed (Fig. 11 & 12) and the sedimentary section 'de-silled'

Within the study area, the total thickness of the Cretaceous based on seismic mapping varies from 3,113 m in the basinal areas to 161 m on the structural highs, with an average thickness of 2,491 m. Other studies looking at the Cretaceous across the FSB have a range of thicknesses from 4.5 to 5 km of sediment (Lamers & Carmichael 1999; Stoker 2016). However, when the igneous material is removed from the Cretaceous, reconstructing it to its true thickness prior to the emplacement of the FSSC, the Cretaceous sedimentary sequence becomes much thinner. For example, in the Nuevo sub-basin, the Cretaceous sequence ranges from 2,883 to 3,672 m, removing the cumulative igneous material would result in a Cretaceous which is up to 1,500 m thinner.

It is important to note that the thickness of the igneous material is not uniform across the study area, with some regions having considerably more igneous material, even across relatively short distances. For example the Nuevo sub-basin is heavily intruded in comparison to the Cambo High, only 2 km away (Fig. 8). This spatially non-uniform nature of intrusion thickness in sub-basins is likely the result of the magma input zones as highlighted by Schofield *et al.* (2015). This work also shows that proximity to half-graben bounding faults results in greater number of intrusions, as these bounding faults are acting as magma conduits for deep input into the basin. The Nuevo sub-basin is the most

heavily intruded sub-basin in the FSB due to a major Cretaceous-Paleocene fault on the south of the Corona Ridge (Fig. 8). This major fault was likely a long-lived magma conduit transferring vast amounts of igneous material into the Nuevo Sub-basin. The difference in the abundance of igneous material across the basin is important to consider as it implies that each sub-basin has a different evolution through time and therefore must treated individually.

Recognition of the potential for a much thinner Cretaceous sequence has some major implications. In particular it suggests that previous estimations of sedimentation rates in the FSB, particularly for the Cretaceous, have been overestimated in areas. Acknowledging that sedimentation rates are much lower during the Cretaceous is essential for understanding the development of Cretaceous phases of rifting along the North Atlantic Margin. Stoker (2016) documents thick accumulations of sediments in the Upper Cretaceous for the Judd (1,583 m) and Flett sub-basins (3,719 m) as evidence of the magnitude of rifting during this period. We note that the time period of the Upper Cretaceous inferred by Stoker (2016) to having the thickest sedimentary sequence and highest sedimentation rates is also the most heavily intruded stratigraphy. Stoker (2016) calculates the sedimentation rate of 73.9 m Ma^{1} within the Flett sub-basin, based on a thickness of 2,551 m of sediment in the Upper Cretaceous. However, accounting for the maximum thickness of igneous material in the Upper Cretaceous from this study, the true thickness of the Upper Cretaceous that Stoker (2016) based calculations on could be up to 800 m thinner, leading to a downward revision of sedimentation rates of 51.3 m Ma^{-1}. Importantly, to correctly estimate sedimentation rates in FSB, heavily intruded sections necessitate correction for the abundant igneous intrusions (de-sill). A further important aspect of the overthickening of the sedimentary sequence by the igneous intrusions would be to understand the uplift effect of the numerous igneous intrusions. There are numerous uplift related unconformities during the Paleocene to Eocene across the FSB which could be related to the uplift associated with the emplacement of these igneous intrusions (Ritchie *et al.* 2011).

Implications of overestimating the sedimentary fill for petroleum system modelling and petroleum exploration

A critical part of hydrocarbon exploration and petroleum system analysis (PSA) is burial history modelling to determine when source rocks generate and expel hydrocarbons (Magoon & Dow 1994). Generation modelling in the FSB has proven problematic as current models indicate that the primary source rock, the Upper Jurassic Kimmerridge Clay Formation (KCF) is post-mature for hydrocarbon generation in the main basinal regions of the FSB and peak generation preceded the deposition of the proven Paleocene reservoirs and trap formation (Scotchman *et al.* 2006). Penetrations on the basin highs such as the Corona Ridge have identified KCF sediments which are immature, but within the basinal areas these are deeply buried. (Scotchman *et al.* 2006). Previous research has evoked different models to account for this discrepancy. Dore *et al.* (1997) and Lamers & Carmichael (1999) describe the peak generation occurring in the late Cretaceous, with early Cretaceous sandstones acting as paleo-accumulations of hydrocarbons before later migration into the Paleogene reservoirs. This theory is known as the "Motel Model". Alternatively, Scotchman *et al.* (2006) argued that the misalignment between hydrocarbon generation and deposition of the reservoirs is due to maturation retardation by overpressures. Both the motel model and the overpressure model invoke an offset between the onset of hydrocarbon generation and the timing of charge into Paleogene reservoirs, but the processes apply to limited geographical areas and are not applicable to the whole basin.

Commonly where sedimentary basins are affected by intrusive igneous activity, a focus has been placed on the direct heating effect that intrusions could have on organic rich sediments and how this could result in local generation of hydrocarbons through direct kerogen cracking (Clayton & Bostick 1985; Bishop & Abbot 1995; Aarnes *et al.* 2011; Muirhead *et al.* 2017). It has often been shown that maturity trends are locally elevated in the host rock surrounding igneous intrusions due the high emplacement temperatures (>1,000 °C for mafic intrusions), often resulting in early generation of hydrocarbons if emplaced within organic-rich shales. However, what has not been considered is the direct thickening and loading effects that the addition of intrusions rapidly overthickening a sequence can have on basin modelling and, in particular, the point at which underlying source rocks begin to generate and expel hydrocarbons.

We propose that a new approach to basin modelling in basins with abundant igneous intrusions is required. We have demonstrated that the total thickness of igneous material in the Cretaceous and lower Paleocene can be as great as >2 km in some parts of the study area. The intrusions could result in overestimation of the implied Cretaceous sedimentation rates and thus overburden thickness, which is the key control influencing source maturation. In the Nuevo sub-basin, where the thickest accumulation of intrusions occurs, the mapped thickness of the Cretaceous is 4.5 km but with as much as 2 km of igneous material. This is critical for basin modelling, as a thicker Cretaceous and lower Paleocene at the time of deposition will result in greater burial of the underlying KCF source rock and therefore earlier onset of hydrocarbon generation. Alternatively, if one restores the basin to its true thickness at the time of deposition, prior to emplacement of intrusions, the onset of generation could occur later. Future hydrocarbon generation modelling across the whole of the Atlantic Margin (and over global basins) should fully account for overthickening, including the greater thickness of igneous material in the basinal areas.

CONCLUSIONS

This study demonstrates that with 3D seismic data it is possible to estimate the thickness of igneous intrusions and estimate the total volume of igneous material in a basin. By estimating the amount of intrusive igneous material in the basin, the findings and implications for basin evolution can be summarised as follows:

- This study shows that for the FSB the cumulative thickness of igneous material within sedimentary sequences in different sub-basins can be as great as 2 km.
- The volume of igneous material ranges from 399 – 22205 km^3, which is comparable to similar seismic based volume estimates, but also highlights that previous studies have overestimated the volume of intrusive igneous material due to less thorough methods, than outlined in this study.
- At the paleo-depth of emplacement for the intrusions in this study, there is reduced porosity in the host rocks due to burial compaction. With limited porosity, we determine that the

accommodation process for the igneous intrusions in the study area is 1:1 uplift of the host rocks ('Jacking-Up' structures) to accommodate the igneous intrusions.

- There is overestimation of the true depositional thickness of the Cretaceous and lower Paleocene because of the additional igneous material. This igneous material was not emplaced into these sediments until 56.5 Ma and has important implications for understanding sedimentation rates and rifting during the Cretaceous and lower Paleocene.
- Reconstructing the basin history to remove this igneous material ("*de-sill*") to get true thicknesses of the host rock sediments is critical for accurate basin modelling. Ignoring this step can result in basin models which do not account for the true geological history when modelling the onset of petroleum generation. This omission leads to improper evaluation of exploration prospects.

In summary, this study shows that igneous intrusions can have significant implications for the understanding of basin evolution. Compared to previous ways that basin models have incorporated igneous intrusion this model shows that intrusions (in relation to timing) can actually change the onset of hydrocarbon generation, rather than accelerate it through direct heating effects. Application of the approach demonstrated in this study would benefit the evaluation of other basins with significant intrusive igneous material to understand the basin evolution and to recognise the petroleum generation and expulsion history of source rocks.

ACKNOWLEDGEMENTS

This study was part of a collaboration between the University of Aberdeen, Siccar Point Energy Ltd and Integrated Geochemical Interpretation (IGI). Siccar Point Energy Ltd are thanked for giving the author permission to publish. Karolina Harvie and Kevin Ward from Petrosys are thanks for their support during the mapping process of the project. The lead author's PhD is funded by JX Nippon Exploration and Production (U.K.) Limited as part of the Volcanic Margin Research Consortium Phase 2. PGS are thanked for allowing the author access to the MegaSurveyPlus and PGS/TGS FSB 2011-12

MultiClient GeoStreamer data and for granting permission to publish this work. Seismic interpretation was carried out using Schlumberger Petrel software. Well log analysis was carried out using Schlumberger Techlog software. Dave Ellis and Victoria Pease are thanked for the comments which greatly improved the revisions of this paper. Well data was obtained from the UK Oil and Gas Authority (OGA) Common Data Access (CDA).

REFERENCES

Aarnes, I., Svensen, H., Connolly, J.A. and Podladchikov, Y.Y., 2010. How contact metamorphism can trigger global climate changes: Modeling gas generation around igneous sills in sedimentary basins. *Geochimica et Cosmochimica Acta*, *74*(24), pp.7179-7195.

Aarnes, I., Fristad, K., Planke, S. and Svensen, H., 2011. The impact of host-rock composition on devolatilization of sedimentary rocks during contact metamorphism around mafic sheet intrusions. *Geochemistry, Geophysics, Geosystems*, *12*(10).

Allen, P.A. and Allen, J.R., 2013. *Basin analysis: Principles and application to petroleum play assessment*. John Wiley & Sons.

Archer, S.G., Bergman, S.C., Iliffe, J., Murphy, C.M. & Thornton, M. 2005. Palaeogene igneous rocks reveal new insights into the geodynamic evolution and petroleum potential of the Rockall Trough, NE Atlantic Margin. Basin Res.,**17**, 171–201.

Bell, B.R. & Butcher, H. 2002. On the emplacement of sill complexes: evidence from the Faroe-Shetland Basin. In: The North Atlantic Igneous Province: Stratigraphy, Tectonic, Volcanic and Magmatic Processes (Ed. by D.W. Jolly & B. Bell) Geol. Soc. London. Spec. Publ., **197**, 307–329.

Bishop, A.N. and Abbott, G.D., 1995. Vitrinite reflectance and molecular geochemistry of Jurassic sediments: the influence of heating by Tertiary dykes (northwest Scotland). *Organic Geochemistry*, *22*(1), pp.165-177.

Clayton, J.L. and Bostick, N.H., 1986. Temperature effects on kerogen and on molecular and isotopic composition of organic matter in Pierre Shale near an igneous dike. *Organic Geochemistry*, *10*(1-3), pp.135-143.

Davies, R., Bell, B.R., Cartwright, J.A. and Shoulders, S., 2002. Three-dimensional seismic imaging of Paleogene dike-fed submarine volcanoes from the northeast Atlantic margin. *Geology*, *30*(3), pp.223-226.

Doré, A.G., Lundin, E.R., Birkeland, O., Eliassen, P.E. and Jensen, L.N., 1997. The NE Atlantic margin; implications of late Mesozoic and Cenozoic events for hydrocarbon prospectivity. *Petroleum Geoscience*, *3*(2), pp.117-131.

Eide, C.H., Schofield, N., Jerram, D.A. and Howell, J.A., 2017a. Basin-scale architecture of deeply emplaced sill complexes: Jameson Land, East Greenland. *Journal of the Geological Society*, *174*(1), pp.23-40.

Eide, C.H., Schofield, N., Lecomte, I., Buckley, S.J. and Howell, J.A., 2017b. Seismic interpretation of sill complexes in sedimentary basins: implications for the sub-sill imaging problem. *Journal of the Geological Society*, pp.jgs2017-096.

Einsele, G., Gieskes, J.M., Curray, J., Moore, D.M., Aguayo, E., Aubry, M.P., Fornari, D., Guerrero, J., Kastner, M., Kelts, K. and Lyle, M., 1980. Intrusion of basaltic sills into highly porous sediments, and resulting hydrothermal activity. *Nature*, *283*(5746), p.441.

Eldholm, O. and Grue, K., 1994. North Atlantic volcanic margins: dimensions and production rates. *Journal of Geophysical Research: Solid Earth*, *99*(B2), pp.2955-2968.

Ellis, D., Passey, S.R., Jolley, D.W. & Bell, B.R. 2009. Transfer zones: the application of new geological information from the Faroe Islands applied to the offshore exploration of intra-basalt and sub-basalt strata. In: Faroe Islands Exploration Conference: Proceedings of the 2nd Conference. Annales Societatis Scientiarum, Færoensis, Supplementum (Ed. by T. Varming & H. Ziska), **50**, 174 -204.

Ellis, D. and Stoker, M.S., 2014. The Faroe–Shetland Basin: A regional perspective from the Paleocene to the present day and its relationship to the opening of the North Atlantic Ocean. *Geological Society, London, Special Publications*, *397*, pp.SP397-1.

Ellwood, B.B. and Watkins, N.D., 1976. Comparison of observed intrusive to extrusive ratios in Iceland and the Troodos Massif with results of experimental emplacement mode analysis of DSDP igneous rocks. *Journal of Geophysical Research*, *81*(23), pp.4152-4156.

Ferguson, D.J., Barnie, T.D., Pyle, D.M., Oppenheimer, C., Yirgu, G., Lewi, E., Kidane, T., Carn, S. and Hamling, I., 2010. Recent rift-related volcanism in Afar, Ethiopia. *Earth and Planetary Science Letters*, *292*(3), pp.409-418.

Gibb, F. & Kanaris-sotiriou, R. 1988. The geochemistry and origin of the Faeroe–Shetland Sill Complex. In: Early Tertiary Volcanism and the Opening of the NE Atlantic (Ed. by A.C. Morton & L.M. Parson) Geol. Soc. Lond. Spec. Publ., **39**, 241–252.

Gluyas, J. and Cade, C.A., 1997. Prediction of porosity in compacted sands.

Grove, C., 2014. *Direct and indirect effects of flood basalt volcanism on reservoir quality sandstone* (Doctoral dissertation, Durham University).

Grove, C., Jerram, D.A., Gluyas, J.G. and Brown, R.J., 2017. Sandstone Diagenesis in Sediment–lava Sequences: Exceptional Examples of Volcanically Driven Diagenetic Compartmentalization in Dune Valley, Huab Outliers, Nw Namibia. *Journal of Sedimentary Research*, *87*(12), pp.1314-1335.

Hardman, J., Schofield, N., Jolley, D., Hartley, A., Holford, S. and Watson, D., 2018. Controls on the distribution of volcanism and intra-basaltic sediments in the Cambo–Rosebank region, West of Shetland. *Petroleum Geoscience*, pp.petgeo2017-061.

Hitchen, K & Ritchie, J.D. 1987. Geological review of the West of Shetland area. In: Petroleum Geology of North West Europe, Brooks, J. and Glennie, K. (eds), 1987, Graham & Trotman, pp 737-749.

Holbrook, W.S., Larsen, H.C., Korenaga, J., Dahl-Jensen, T., Reid, I.D., Kelemen, P.B., Hopper, J.R., Kent, G.M., Lizarralde, D., Bernstein, S. and Detrick, R.S., 2001. Mantle thermal structure and active upwelling during continental breakup in the North Atlantic. *Earth and Planetary Science Letters*, *190*(3), pp.251-266.

Holford, S.P., Schofield, N., Jackson, C.A.-L., Magee, C., Green, P.F. & Duddy, I.R. 2013. Impacts of igneous intrusions on source and reservoir potential in prospective sedimentary basins along the western Australian continental margin. In: The Sedimentary Basins of Western Australia IV (Ed. by M.

Keep & S.J. Moss), Proceedings of the Petroleum Exploration Society of Australia Symposium, Perth, WA.

Hutton, D.H.W., 2009. Insights into magmatism in volcanic margins: bridge structures and a new mechanism of basic sill emplacement–Theron Mountains, Antarctica. *Petroleum Geoscience*, *15*(3), pp.269-278.

Jackson, C.A., Schofield, N. and Golenkov, B., 2013. Geometry and controls on the development of igneous sill–related forced folds: A 2-D seismic reflection case study from offshore southern Australia. *Bulletin*, *125*(11-12), pp.1874-1890.

Jerram, D.A., Davis, G.R., Mock, A., Charrier, A. and Marsh, B.D., 2010. Quantifying 3D crystal populations, packing and layering in shallow intrusions: A case study from the Basement Sill, Dry Valleys, Antarctica. *Geosphere*, *6*(5), pp.537-548.

Jolley, D.W. and Bell, B.R., 2002. The evolution of the North Atlantic Igneous Province and the opening of the NE Atlantic rift. *Geological Society, London, Special Publications*, *197*(1), pp.1-13.

Kiyosugi, K., Connor, C.B., Wetmore, P.H., Ferwerda, B.P., Germa, A.M., Connor, L.J. and Hintz, A.R., 2012. Relationship between dike and volcanic conduit distribution in a highly eroded monogenetic volcanic field: San Rafael, Utah, USA. *Geology*, *40*(8), pp.695-698.

Lamers, E. & Carmichael, S.M.M. 1999. The Paleocene deepwater sandstone play west of Shetland. In: Petroleum Geology of Northwest Europe: Proceedings of the 5th Conference (Ed. By A.J. Fleet & S.A.R. Boldy), pp. 645–659. The Geological Society, London.

Magee, C., Briggs, F. and Jackson, C.A., 2013. Lithological controls on igneous intrusion-induced ground deformation. *Journal of the Geological Society*, *170*(6), pp.853-856.

Magee, C., Muirhead, J.D., Karvelas, A., Holford, S.P., Jackson, C.A., Bastow, I.D., Schofield, N., Stevenson, C.T., McLean, C., McCarthy, W. and Shtukert, O., 2016. Lateral magma flow in mafic sill complexes. *Geosphere*, *12*(3), pp.809-841.

Magoon, L.B. and Dow, W.G., 1991. The petroleum system-from source to trap. *AAPG Bulletin (American Association of Petroleum Geologists);(United States)*, *75*(CONF-910403--).

Mark, N.J., Schofield, N., Pugliese, S., Watson, D., Holford, S., Muirhead, D., Brown, R. and Healy, D., 2017. Igneous intrusions in the Faroe Shetland basin and their implications for hydrocarbon exploration; new insights from well and seismic data. *Marine and Petroleum Geology*.

Mudge, D. C. 2014. Regional controls on Lower Tertiary sandstone distribution in the North Sea and NE Atlantic margin basins. *In*: McKie, T. Rose, P. T. S. Hartley, A. J. Jones, D. W. & Armstrong, T. L. (eds) *Tertiary Deep-Marine Reservoirs of the North Sea Region*. Geological Society, London, Special Publications, **403**, 17-42.

Muirhead, D.K., Bowden, S.A., Parnell, J. and Schofield, N., 2017. Source rock maturation owing to igneous intrusion in rifted margin petroleum systems. *Journal of the Geological Society*, 011.

Planke, S., Rasmussen, T., Rey, S.S. and Myklebust, R., 2005, January. Seismic characteristics and distribution of volcanic intrusions and hydrothermal vent complexes in the Vøring and Møre basins. In *Geological Society, London, Petroleum Geology Conference series* (Vol. 6, No. 1, pp. 833-844). Geological Society of London.

Pryor, W.A., 1973. Permeability-porosity patterns and variations in some Holocene sand bodies. *AAPG Bulletin*, *57*(1), pp.162-189.

Reynolds, P., Holford, S., Schofield, N. and Ross, A., 2018. The importance of subsurface lithology in controlling magma storage v. eruption: an example from offshore southern Australia. *Journal of the Geological Society*, pp.jgs2017-109.

Richardson, J.A., Connor, C.B., Wetmore, P.H., Connor, L.J. and Gallant, E.A., 2015. Role of sills in the development of volcanic fields: Insights from lidar mapping surveys of the San Rafael Swell, Utah. *Geology*, *43*(11), pp.1023-1026.

Ritchie, J.D., Ziska, H., Johnson, H. & Evans, D., Eds. 2011. Geology of the Faroe-Shetland Basin and Adjacent Areas. British Geological Survey, Nottingham, UK. 317 pp (RR/11/ 001).

Roberts, A.W., White, R.S. and Christie, P.A.F., 2009. Imaging igneous rocks on the North Atlantic rifted continental margin. *Geophysical Journal International*, *179*(2), pp.1024-1038.

Senger, K., Millett, J., Planke, S., Ogata, K., Eide, C.H., Festøy, M., Galland, O. and Jerram, D.A., 2017. Effects of igneous intrusions on the petroleum system: a review. *First Break*, *35*(6), pp.47-56.

Schofield, N., Heaton, L., Holford, S., Archer, S., Jackson, C. & Jolley., D.W. 2012a. Seismic imaging of 'Broken-Bridges': linking seismic to outcrop-scale investigations of intrusive magma lobes. J. Geol. Soc., 169, 421–426.

Schofield, N.J., Brown, D.J., Magee, C. and Stevenson, C.T., 2012b. Sill morphology and comparison of brittle and non-brittle emplacement mechanisms. *Journal of the Geological Society*, *169*(2), pp.127-141.

Schofield, N., Holford, S., Millet, J., Brown, D., Jolley, D., Passey, S. R., Muirhead, D., Grove, C., Magee, C., Murray, J., Hole, M., Jackson, C. A.-L. & Stevenson, C. 2015. Regional magma plumbing and emplacement mechanisms of the Faroe-Shetland Sill Complex: implications for magma transport and petroleum systems within sedimentary basins. *Basin Research*, first published online November **19**, 2015, http://doi.org/10.1111/ bre.12164.

Schofield, N., Jolley, D., Holford, S., Archer, S., Watson, D., Hartley, A., Howell, J., Muirhead, D., Underhill, J. and Green, P., 2017. Challenges of future exploration within the UK Rockall Basin. In *Geological Society, London, Petroleum Geology Conference series* (Vol. 8, pp. PGC8-37). Geological Society of London.

Scotchman, I.C., 2001. Petroleum geochemistry of the Lower and Middle Jurassic in Atlantic margin basins of Ireland and the UK. *Geological Society, London, Special Publications*, *188*(1), pp.31-60.

Scotchman, I.C., Carr, A.D. and Parnell, J., 2006. Hydrocarbon generation modelling in a multiple rifted and volcanic basin: a case study in the Foinaven Sub-basin, Faroe–Shetland Basin, UK Atlantic margin. *Scottish Journal of Geology*, *42*(1), pp.1-19.

Sheriff, R.E. and Geldart, L.P., 1995. *Exploration seismology*. Cambridge university press.

Simm, R. and Bacon, M., 2014. *Seismic Amplitude: An interpreter's handbook*. Cambridge University Press.

Smallwood, J.R. & Maresh, J. 2002. The properties, morphology and distribution of igneous sills: modelling, borehole data and 3D seismic data from the Faeroe-Shetland area. In: The North Atlantic Igneous Province: Stratigraphy, Tectonic, Volcanic and Magmatic Processes (Ed. by D.W. Jolley & B.R. Bell) Geol. Soc. London. Spec. Publ., **197**, 271–306.

781 Sørensen, A.B., 2003. Cenozoic basin development and stratigraphy of the Faroes area. *Petroleum*
782 *Geoscience*, *9*(3), pp.189-207.
783
784 Stoker, M.S., 2016. Cretaceous tectonostratigraphy of the Faroe–Shetland region. *Scottish Journal of*
785 *Geology*, *52*(1), pp.19-41.
786
787 Storey, M., Duncan, R.A. and Tegner, C., 2007. Timing and duration of volcanism in the North Atlantic
788 Igneous Province: implications for geodynamics and links to the Iceland hotspot. *Chemical*
789 *Geology*, *241*(3-4), pp.264-281.
790
791 Svensen, H., Corfu, F., Polteau, S., Hammer, Ø. and Planke, S., 2012. Rapid magma emplacement in the
792 Karoo large igneous province. *Earth and Planetary Science Letters*, *325*, pp.1-9.
793
794 Thomson, K. and Hutton, D., 2004. Geometry and growth of sill complexes: insights using 3D
795 seismic from the North Rockall Trough. *Bulletin of Volcanology*, *66*(4), pp.364-375.
796
797 Thomson, K. & Schofield, N. 2008. Lithological and structural controls on the emplacement and
798 morphology of sills in sedimentary basins, Structure and Emplacement of High-Level Magmatic Systems.
799 Geol. Soc. Lond. Spec. Publ., 302, 31–44.
800
801 Valentine, G.A. and Perry, F.V., 2007. Tectonically controlled, time-predictable basaltic volcanism from
802 a lithospheric mantle source (central Basin and Range Province, USA). *Earth and Planetary Science*
803 *Letters*, *261*(1-2), pp.201-216.
804
805 White, R. & McKenzie, D. 1989. Magmatism at Rift Zones: The Generation of Volcanic Continental
806 Margins and Flood Basalts. *Journal of Geophysical Research*, **94**, 7685-7729.
807
808 White, S.M., Crisp, J.A. and Spera, F.J., 2006. Long-term volumetric eruption rates and magma
809 budgets. *Geochemistry, Geophysics, Geosystems*, *7*(3).
810
811 Widess, M.B., 1973. How thin is a thin bed?. *Geophysics*, *38*(6), pp.1176-1180.
812
813 **FIGURE CAPTIONS**

814 Figure 1: a) Structural elements map of the Faroe-Shetland Basin, with outline of 3D seismic coverage
815 used in this study, intrusions mapped in this study shown in purple and the wells that penetrated
816 intrusions highlighted in black. b) detailed map showing the outline of the study area and the key
817 structural features of the study area. Figure adapted from Ellis *et al.* 2009; Mudge 2014 and Schofield
818 *et al.* 2015.

819 Figure 2: Seismic line from the FSB showing the typical seismic response of mafic intrusions. Mafic
820 intrusions are characterised in seismic data as laterally discontinuous bright reflectors. Igneous
821 intrusion imaged within the seismic line is represented by a single tuned reflector. Seismic data
822 courtesy of PGS (FSB MegasSurvey Plus).

823 Figure 3: Seismic tuning wedge model demonstrating the concepts of seismic resolution and seismic
824 detectability. λ/4 (λ: lambda) represents the seismic resolution and calculates a thickness of 86 m base
825 on an interval velocity of 5500 m/s for a doleritic intrusion and a seismic frequency of 15.9 Hz using
826 a Ricker wavelet.. λ/8 calculates a thickness of 43 m and λ/30 calculates a thickness of 11.5 m. a)
827 example of igneous intrusions from the seismic data used in this study showing the tuning effect as the
828 intrusion becomes thinner and the top and base reflectors constructively interfere. b) wedge model
829 and resulting seismogram, intrusion is a dolerite with an interval velocity of 5500 m/s within a claystone
830 with an interval velocity of 3048 m/s. c) amplitude versus wedge thickness demonstrating that as the

top and base intrusions reflectors begin to constructively interfere, tuning occurs and the amplitude increases, as the wedge becomes thinner the amplitude decreases. Seismic data is courtesy of PGS (FSB MegaSurvey Plus).

Figure 4: a) seismic through the 205/10-2B well showing three reflectors which represent only three of the igneous intrusions encountered in the well, also shown is the well log which shows the total 44 intrusions that the well actually encountered. b) table showing the true thickness of the intrusions reflectors identified in seismic and the different methods for estimating the thickness based on the tuning wedge model. Seismic data is courtesy of PGS (FSB MegasSurvey Plus).

Figure 5: a) seismic line through the 205/10-2B well and lithology log of all the intrusions encountered in the well. b) logs showing the number of intrusions encountered by the well which can be imaged in seismic versus the intrusions in the well which are unresolvable in the seismic data c), this produces a relationship of 1:1.6 for intrusions which can be imaged vs intrusions which are unimaged. Taking this workflow and applying it to all the wells within the study area produces a relationship of 1:1.4 for intrusions which can be imaged vs intrusions which are unimaged. Using this relationship it is possible to infer the amount of additional igneous material in seismic where there is no well data. Seismic data is courtesy of PGS (FSB MegasSurvey Plus).

Figure 6: Seismic line demonstrating how it is possible to apply the 1:1.4 relationship for imaged to unimaged intrusions to regions of the study area which have no well data to constrain how much additional igneous material there is which is not detected in the seismic data. Seismic data courtesy of PGS (FSB MegasSurvey Plus).

Figure 7: a) map of the study area showing all the mapped intrusions and their thickness estimate based on λ/4 derived from the tuning wedge model. b) map of the study area showing all the mapped intrusions and their thickness estimate based on λ/8 derived from the tuning wedge model. c) map of the study area showing all the mapped intrusions and their thickness estimate based on λ/4 derived from the tuning wedge model, plus the addition of unimaged material. d) map of the study area showing all the mapped intrusions and their thickness estimate based on λ/8 derived from the tuning wedge model. Seismic lines show the numerous stacked intrusions in the Nuevo sub-basin and Flett sub-basins. Seismic data courtesy of PGS (FSB MegasSurvey Plus & PGS/TGS FSB 2011-12 MultiClient Geostreamer).

Figure 8: Detailed structural elements map of the study area showing all the mapped intrusions and their thickness estimate based on λ/4 + plus the addition of unimaged material based on the well relationship. Map shows how sub-basins such as the Nuevo and Flett sub-basin are heavily intruded and generally the basinal highs have fewer intrusions.

Figure 9: Conceptual diagram illustrating the different mechanisms that host rocks accommodate intrusion emplacement in the subsurface. With depth ductile accommodation processes such as host rock deformation becomes less common and at depths greater than 2 km brittle accommodation processes are dominant, such as 1:1 uplift. Figure adapted from Schofield *et al.* 2012b.

Figure 10: a) porosity and ability for intrusions to be accommodated via pore space collapses versus depth for shales, along with the paleo-depth of emplacement for the igneous intrusions mapped in the study area. Shale apparent porosity vs depth from Allen & Allen (2013). This demonstrates that for the average paleo-depth of emplacement for Upper Cretaceous hosted intrusions (UC) the porosity of the host rock would be 4-25% and with 4-25% of the intrusion thickness accommodated by pore space collapse. b) schematic demonstrating how the intrusions in the study area would be accommodated at different depths in the subsurface.

Figure 11: Schematic illustrating the overthickening of the basin fill by igneous intrusions and the reconstruction of the section to its true thickness prior to emplacement of igneous intrusions.

Figure 12: Digitised composite log through the 205/10-2B well showing the 44 intrusions and their cumulative thickness. Removing all this igneous material (*"de-sill"*) to account for the overthickneing results in the Cretaceous section of the well changing from 3240 m thick post emplacement to 2892 m thick when the intrusions have been removed. The restoration of this section to its true thickness could potentially have important implications for basin modelling.

figure

Click here to access/download;figure;Figure 1.jpg

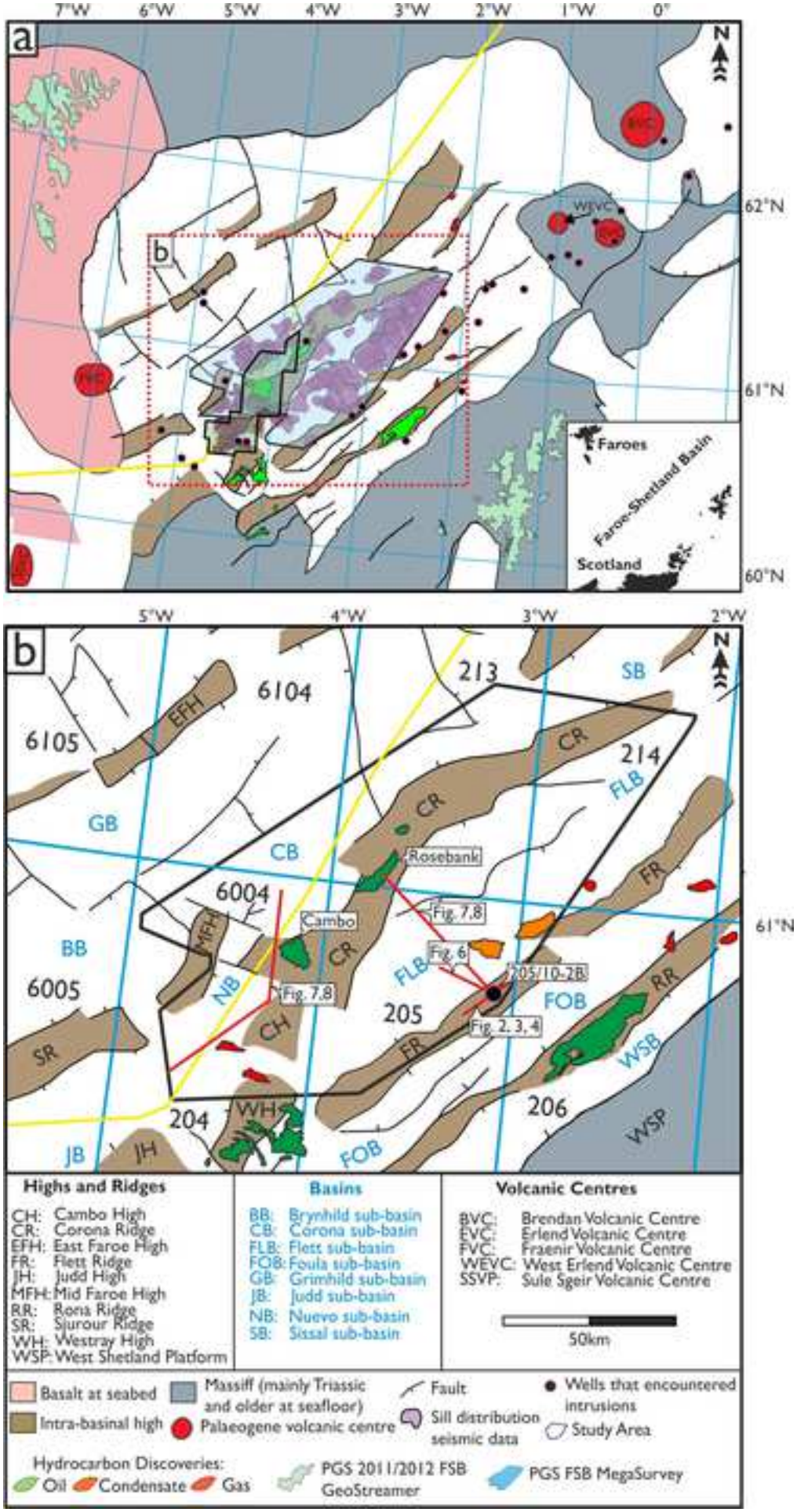

figure

Click here to access/download;figure;Figure 2.jpg

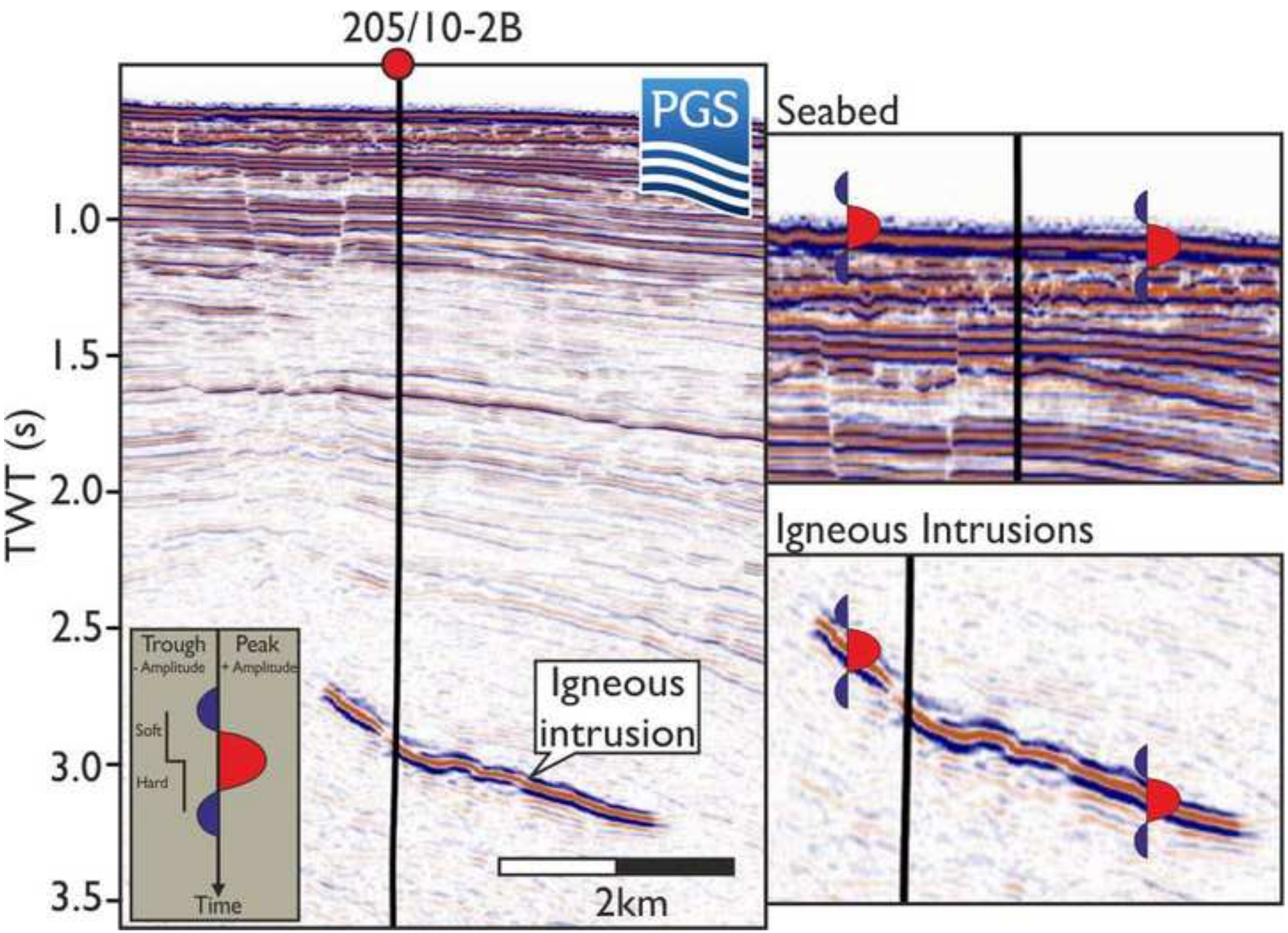

figure

Click here to access/download;figure;Figure 3.jpg

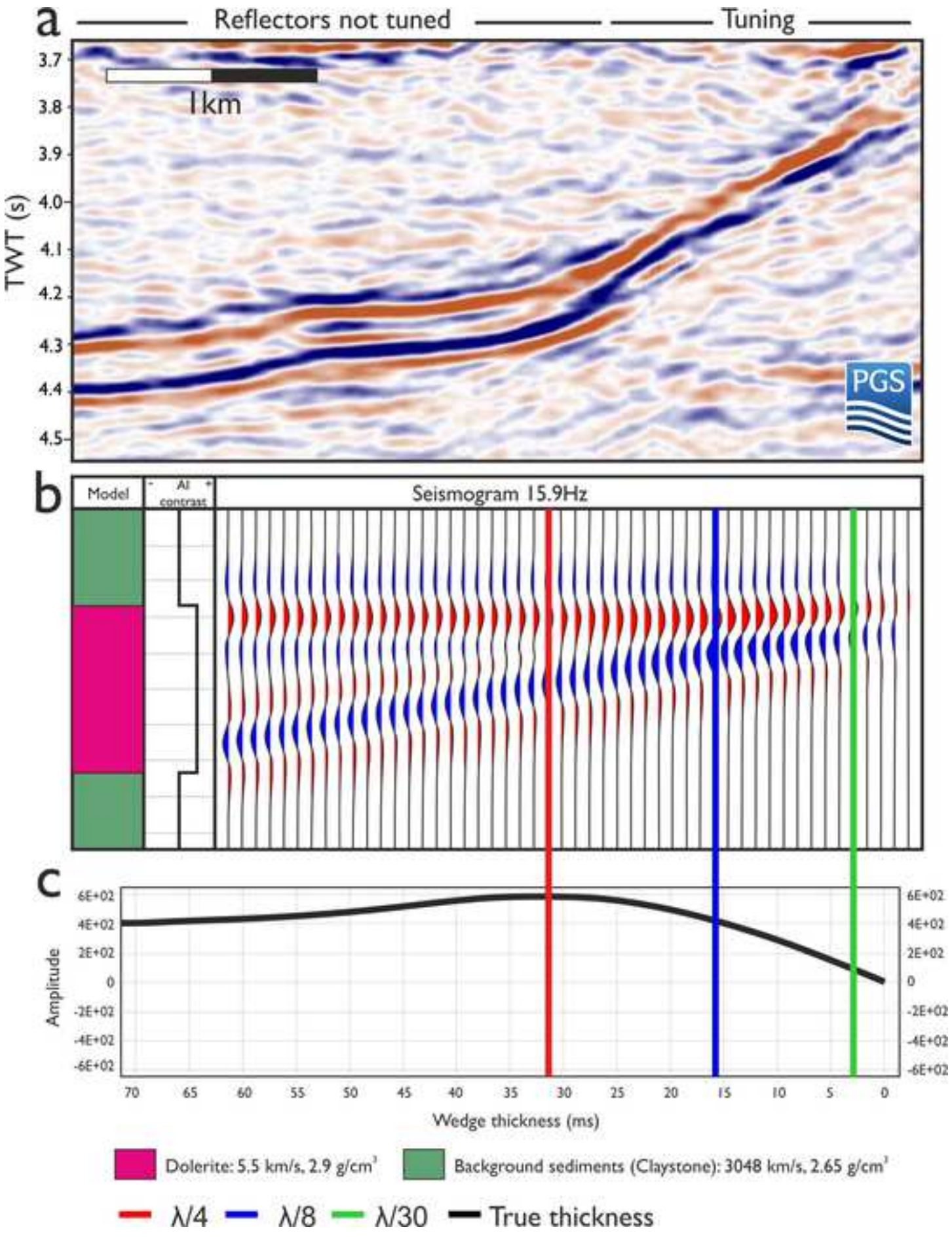

figure

Click here to access/download;figure;Figure 4.jpg

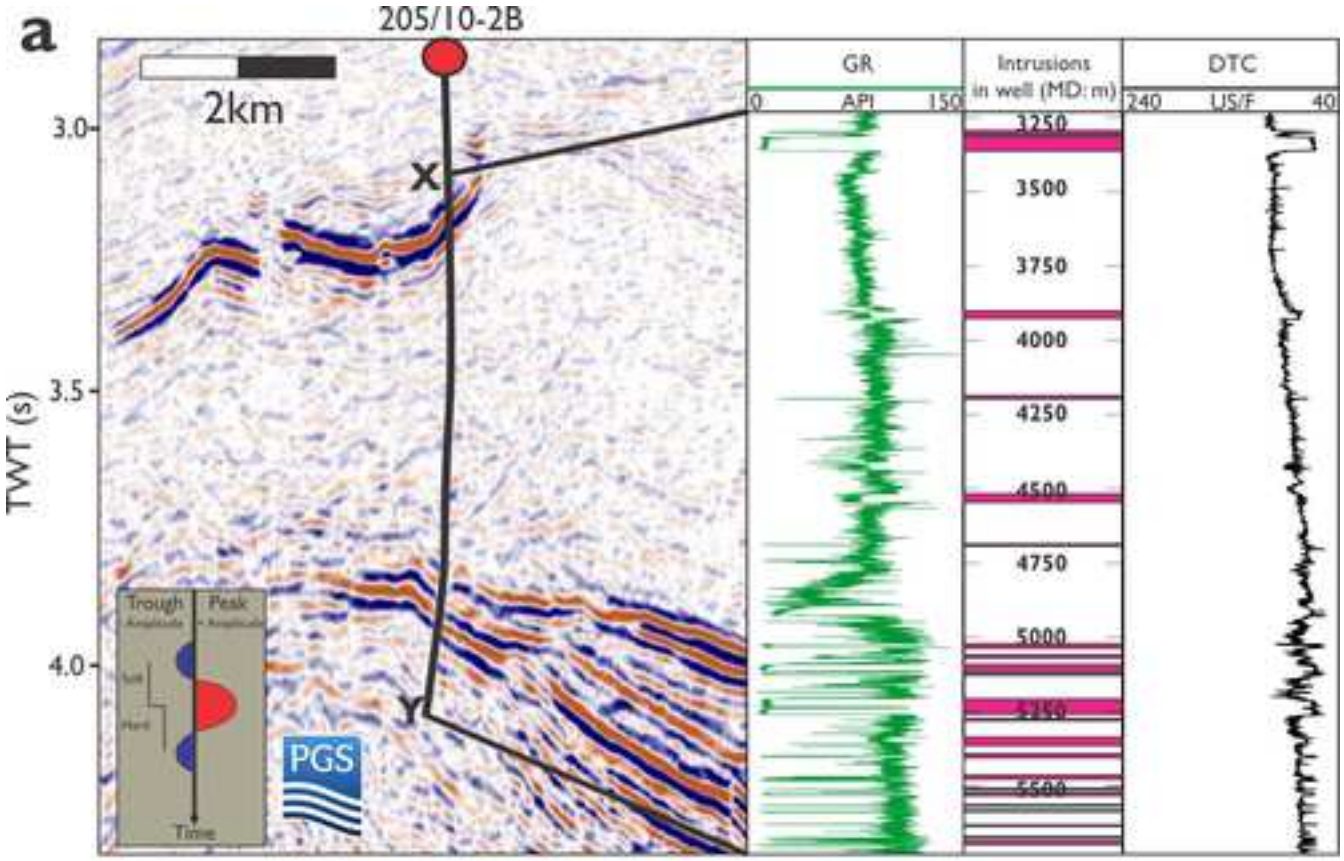

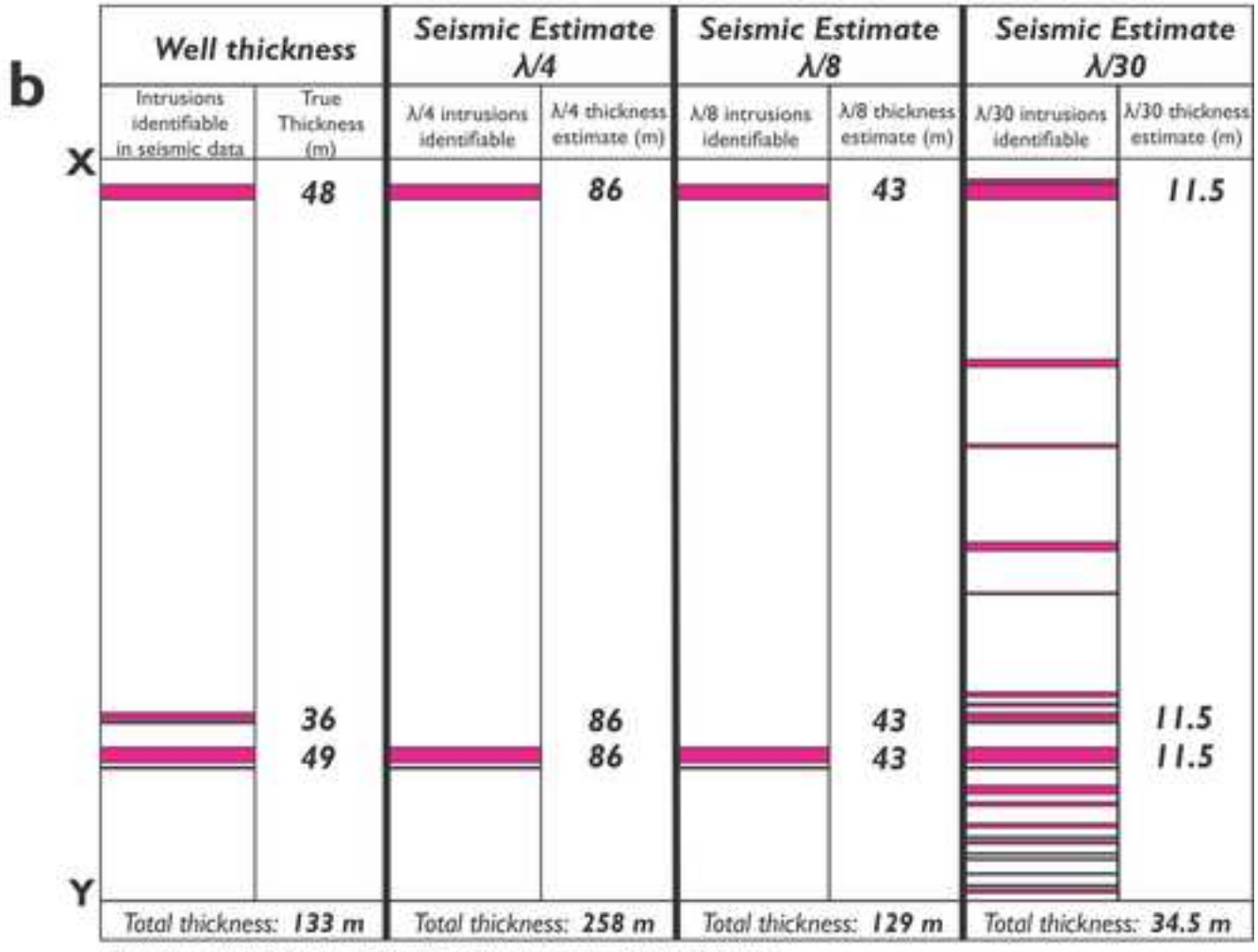

Frequency 15.9 Hz, Dolerite interval velocity 5.5 km/s

figure

Click here to access/download;figure;Figure 5.jpg

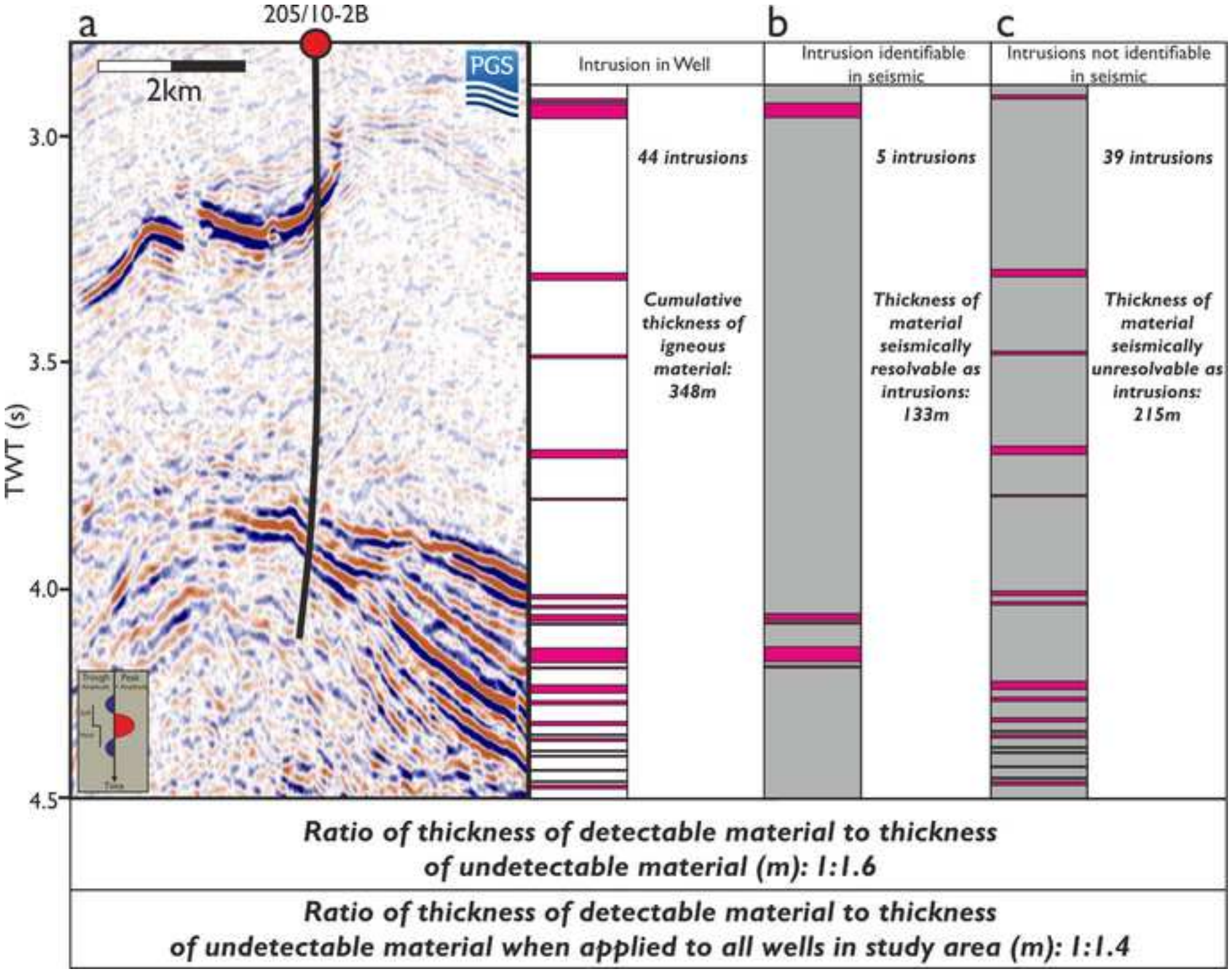

figure

Click here to access/download;figure;Figure 6.jpg

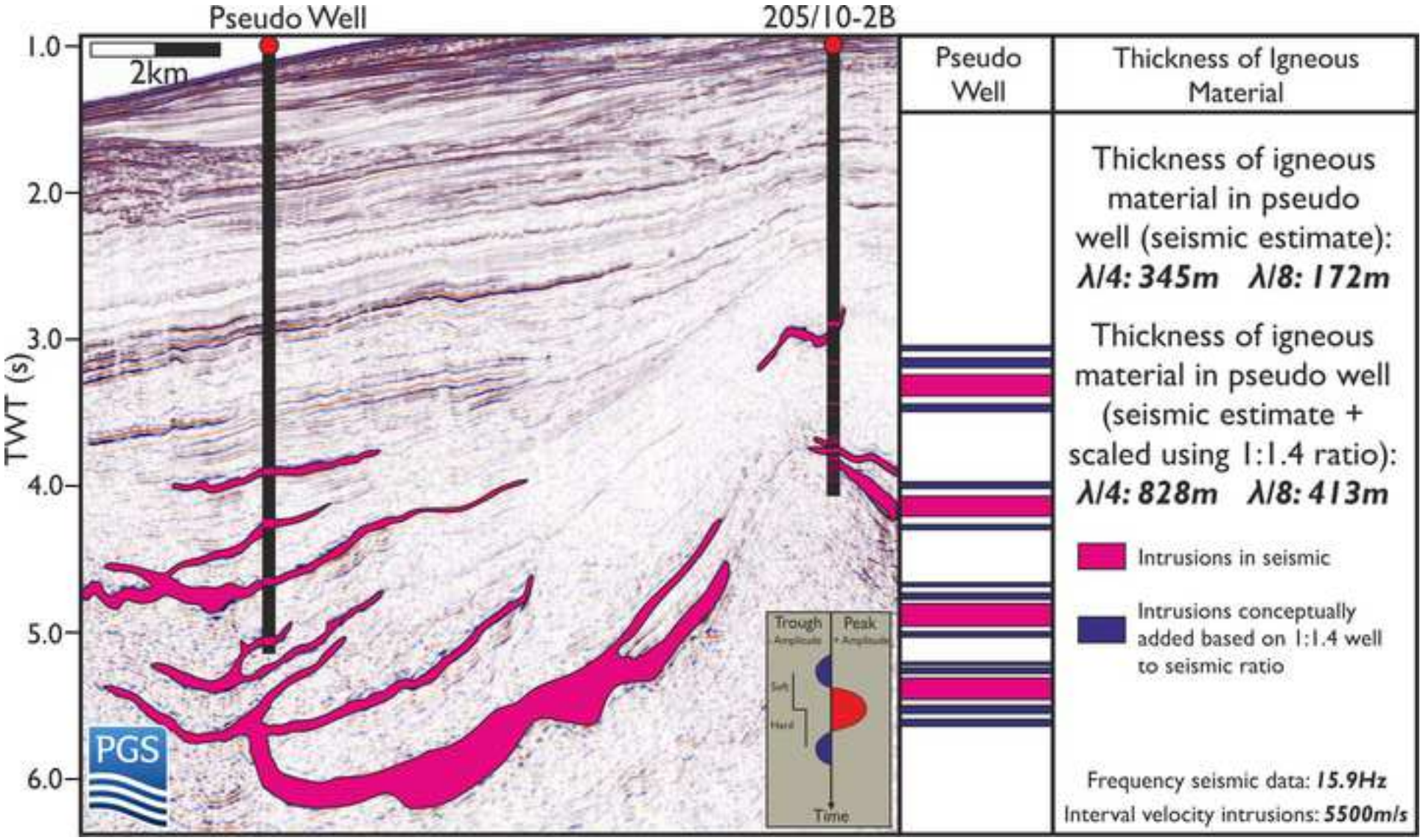

figure

Click here to access/download;figure;Figure 7.jpg

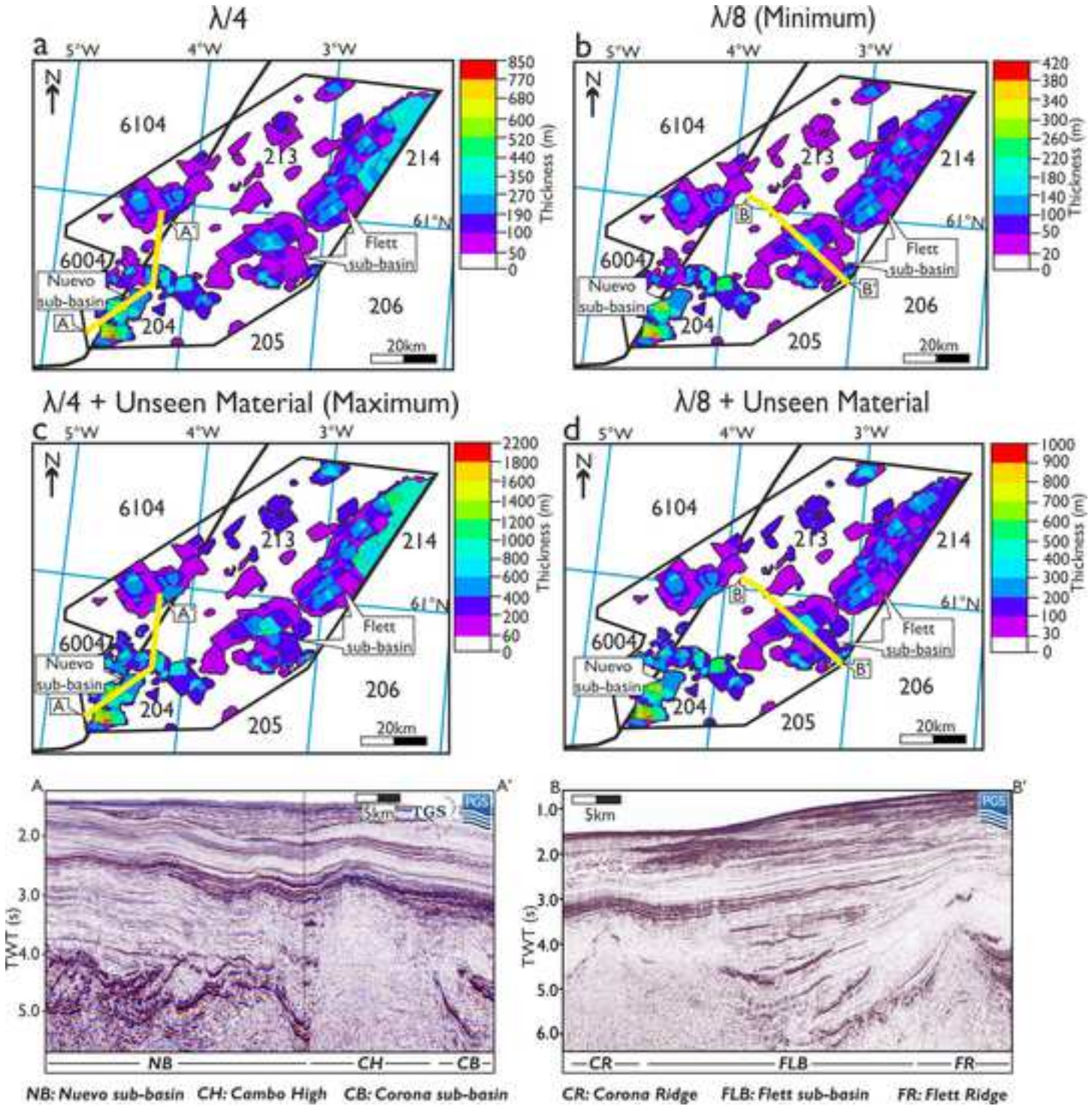

figure

Click here to access/download;figure;Figure 8.jpg

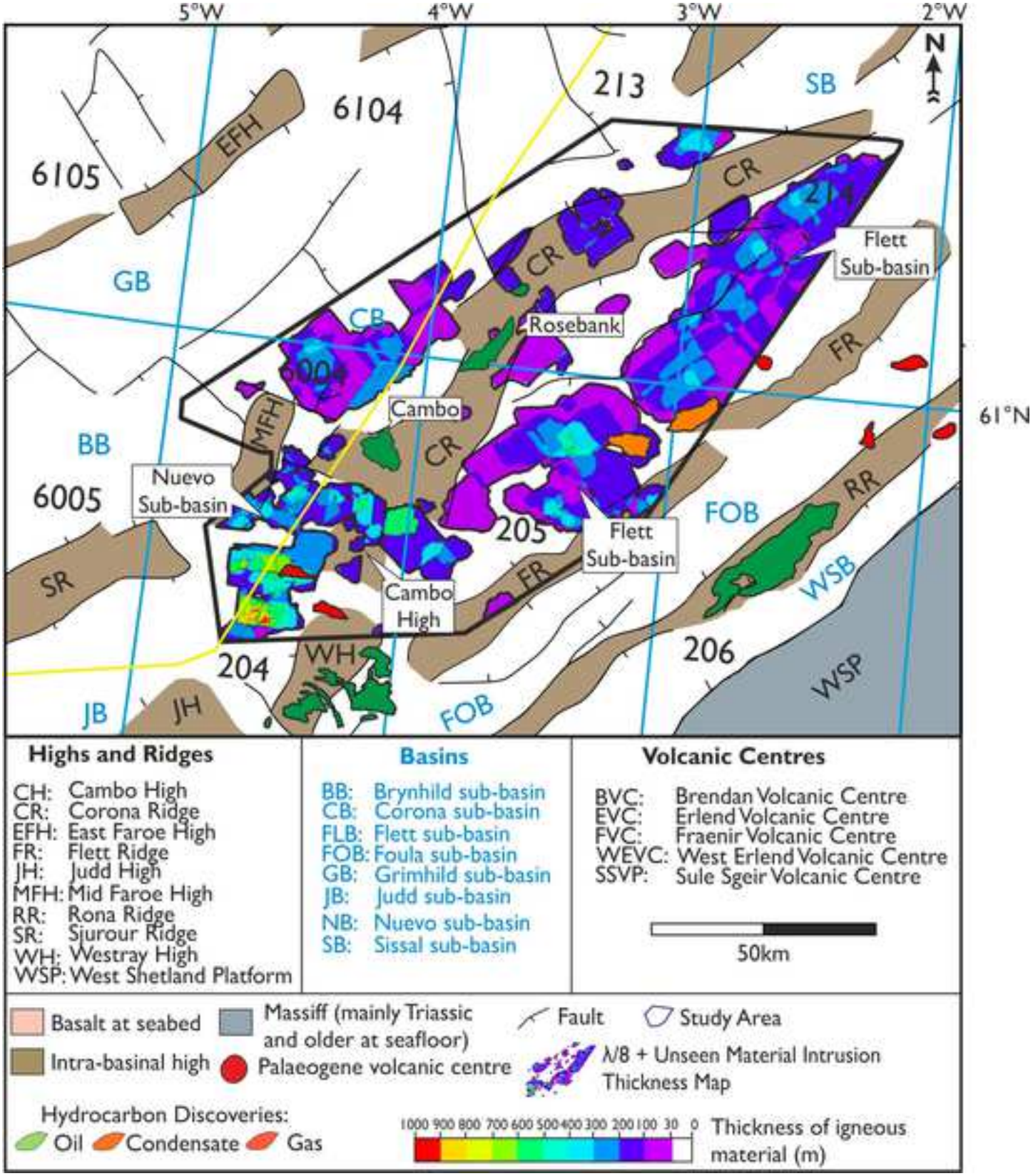

figure

Click here to access/download;figure;Figure 9.jpg

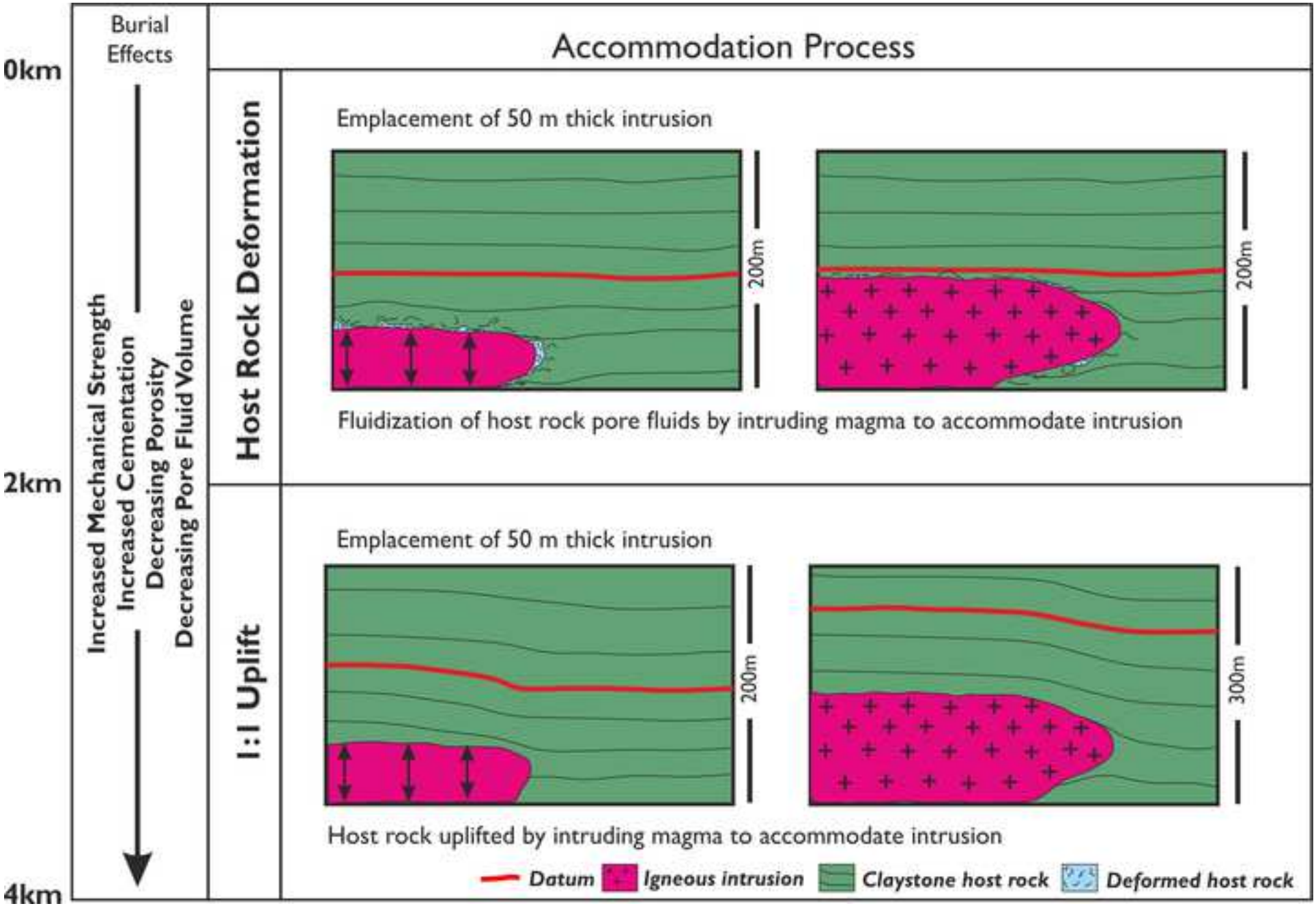

figure

Click here to access/download;figure;Figure 10.jpg

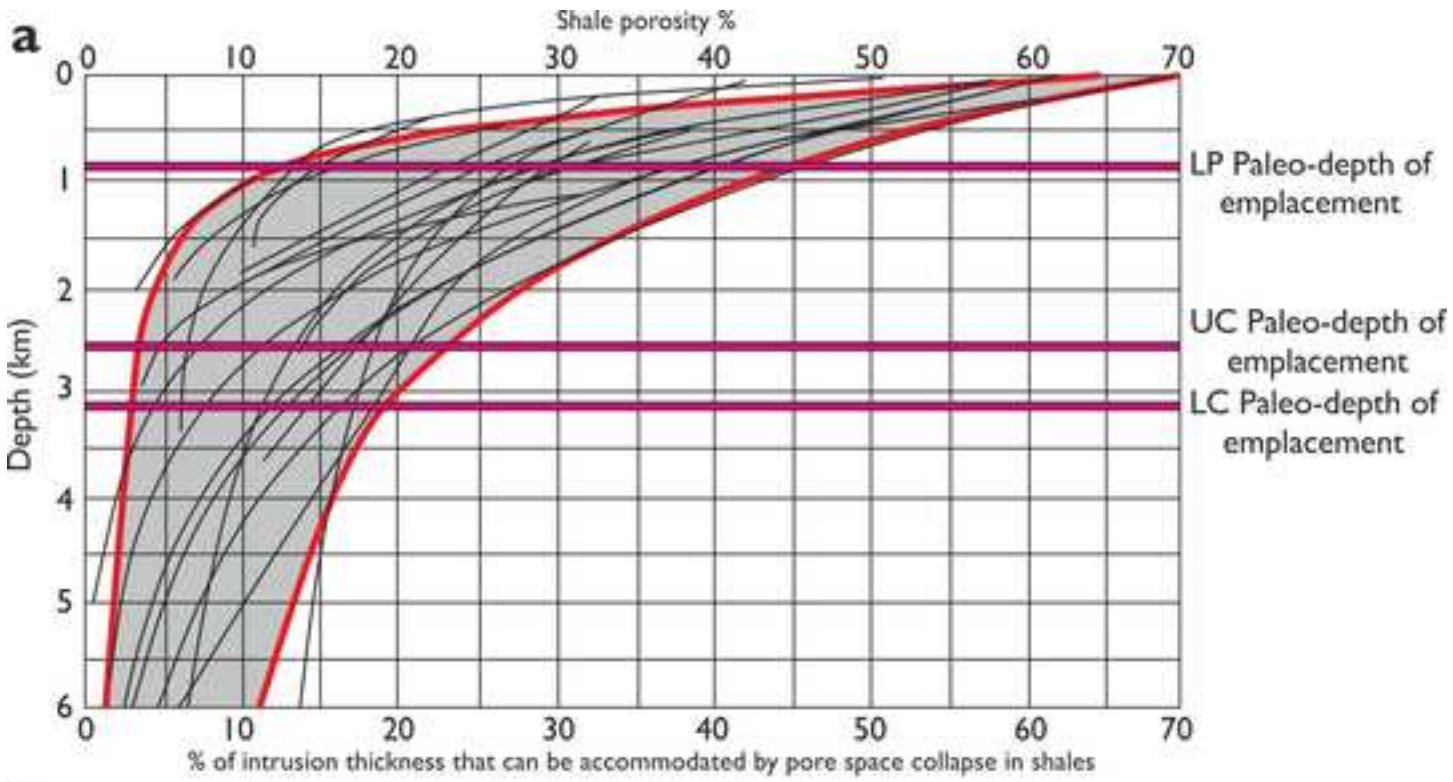

b

LP: Lower Paleocene, **UC:** Upper Cretaceous, **LC:** Lower Cretaceous

Average paleo-depth of emplacement for the Lower Paleocene: 850 m, 12-45% shale porosity

Average paleo-depth of emplacement for the Upper Cretaceous: 2500 m, 4-25% shale porosity

Average paleo-depth of emplacement for the Lower Cretaceous: 3276 m, 3-18% shale porosity

Intrusion of a 50 m thick sill at 800 m subsurface into a shale with 30% porosity

35 m vertical uplift
15 m accommodated by pore space collapse

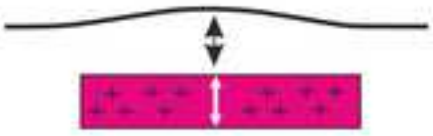

Intrusion of a 50 m thick sill at 2.5 km subsurface into a shale with 10% porosity

45 m vertical uplift
5 m accommodated by pore space collapse

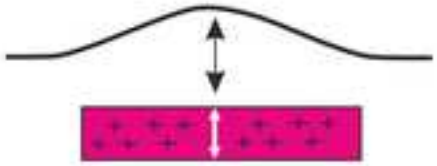

figure

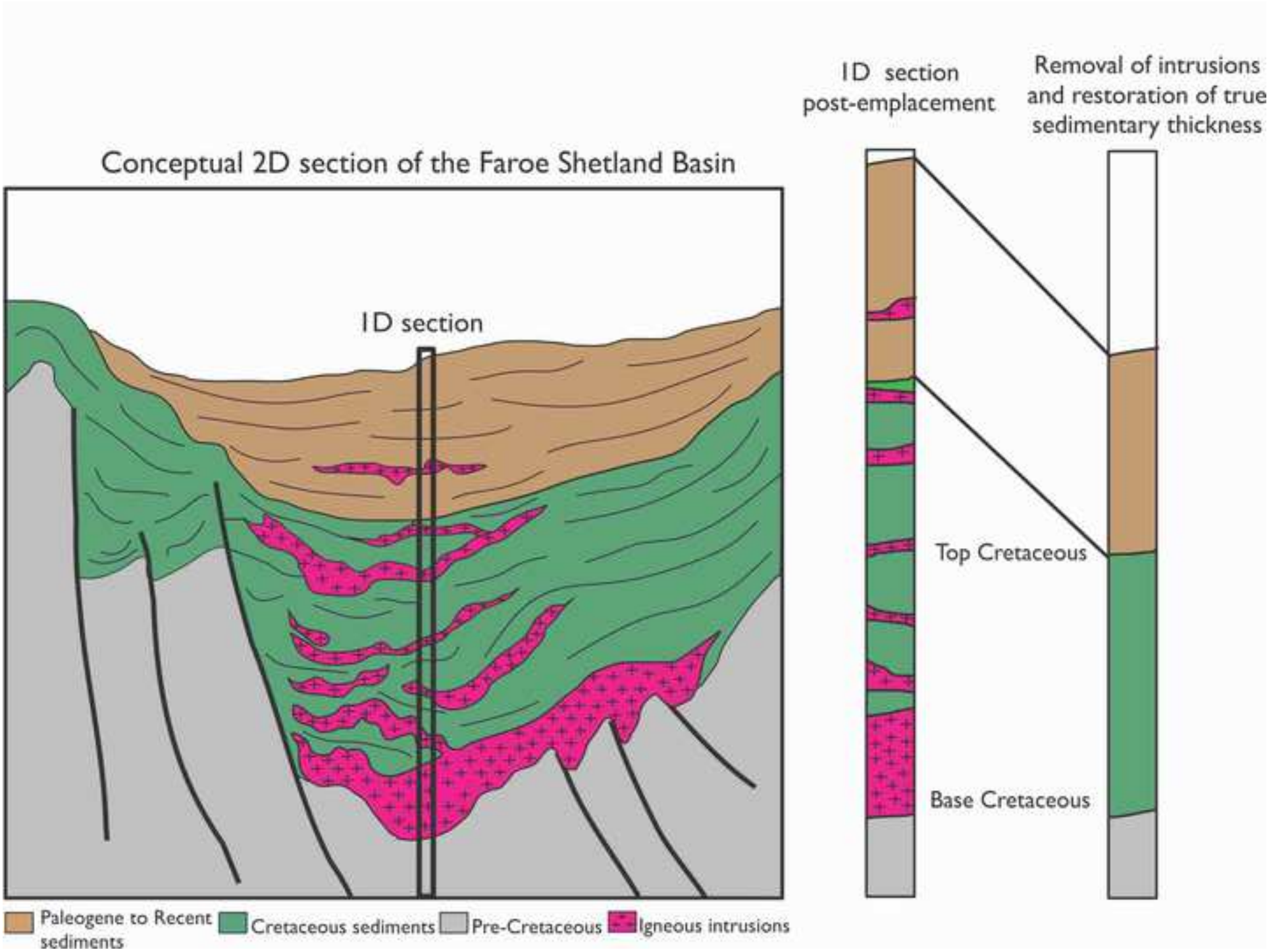

figure

Click here to access/download;figure;Figure 12.jpg